Contrasting impacts of humidity on the ozonolysis of monoterpenes: insights into the multi-generation chemical mechanism

Shan Zhang, Lin Du*, Zhaomin Yang, Narcisse Tsona Tchinda, Jianlong Li, Kun Li*

Environment Research Institute, Shandong University, Qingdao 266237, China.

Correspondence to: Lin Du (lindu@sdu.edu.cn) and Kun Li (kun.li@sdu.edu.cn)

Abstract. Secondary organic aerosol (SOA) formed from the ozonolysis of biogenic monoterpenes is a major source of atmospheric organic aerosol. It has been previously found that relative humidity (RH) can influence the SOA formation from some monoterpenes, yet most studies only observed the increase or decrease in SOA yield without further explanations of molecular-level mechanisms. In this study, we chose two structurally different monoterpenes (limonene with an endocyclic double bond and an exocyclic double bond, Δ^3-carene with only an endocyclic double bond) to investigate the effect of RH in a set of oxidation flow reactor experiments. We find contrasting impacts of RH on the SOA formation: limonene SOA yield increases by ~100% as RH increases, while there is a slight decrease in Δ^3-carene SOA yield. By analyzing SOA chemical composition and reaction mechanisms, the enhancement in limonene SOA yield can be attributed to the water-influenced reactions after ozone attack on the exocyclic double bond of limonene, which leads to the increment of lower volatile organic compounds under high RH condition. However, as Δ^3-carene only has an endocyclic double bond, it cannot undergo such reactions. This hypothesis is further proved by the SOA yield enhancement of β-caryophyllene, a sesquiterpene that also has an exocyclic double bond. These results greatly improve our understanding of how water vapor influences the ozonolysis of biogenic organic compounds and subsequent SOA formation processes.

1 Introduction

Secondary organic aerosol (SOA), as an important type of ambient fine particulate matter (PM$_{2.5}$: aerosols with aerodynamic diameter $\leq$ 2.5 µm) (Guo et al., 2014; Huang et al., 2014), has caused a series of negative impacts on human health (Pye et al., 2021), air quality (Zhang et al., 2016) and global climate (Levy et al., 2013). SOA produced from the oxidation of biogenic volatile organic compounds (BVOCs) is a major component of SOA in heavy forest regions during summer (Sindelarova et al., 2014; Ahmadov

et al., 2012), and contributes by a large fraction (~40%-80%) to global OA budget (Cholakian et al., 2019).

Monoterpenes, mostly emitted from coniferous trees, account for ~11% in total BVOCs (Sindelarova et al., 2014; Kanakidou et al., 2005). Limonene is one of the most abundant monoterpenes, with the annual emission budget of 11.4 Tg yr^{-1} (Guenther et al., 2012). Apart from the biogenic source, limonene can also be released from the indoor emission, mainly from essential oils (Ravichandran et al., 2018; De Matos et al., 2019; Mot et al., 2022). Limonene has an endocyclic double bond and an exocyclic double bond, and is thus more reactive than other monoterpenes towards oxidants such as ozone (O_3), hydroxyl radical (OH), and nitrate radical (NO_3) (Chen and Hopke, 2010; Atkinson and Arey, 2003). Δ^3-carene is another kind of monoterpene that dominates the monoterpene emission from Scots pine (Bäck et al., 2012). Different from limonene, Δ^3-carene contains only one endocyclic double bond, which is similar to most other monoterpenes.

Ozonolysis is an important reaction pathway for limonene and Δ^3-carene. Although reactions with OH and NO_3 are faster than that with O_3 for both two monoterpenes (Atkinson, 1991; Khamaganov and Hites, 2001; Chen et al., 2015; Shaw et al., 2018), the atmospheric concentration of the latter monoterpene is much higher than that of the former (Sbai and Farida, 2019). The contributions of O_3-reactions with limonene and Δ^3-carene to tropospheric degradation are 47% and 24%, respectively, in the daytime (Ziemann and Atkinson, 2012). In pristine areas where NO_3 concentration is very low, ozonolysis is also the dominant fate for limonene and Δ^3-carene in the nighttime. In addition, it has been previously found that the ozonolysis of monoterpenes can produce more extremely low volatility products than OH-initiated oxidation, which contributes by a large fraction to the SOA production (Jokinen et al., 2015). For either limonene or Δ^3-carene, the first step for ozonolysis is attacking on the endocyclic double bond to form two types of stabilized Criegee intermediates (sCI) with low energy (Fig. S1) (Drozd and Donahue, 2011; Chen et al., 2019). The sCI will then trigger a series of chemical reactions, like isomerization, decomposition and addition reactions. Correspondingly, the major components in Δ^3-carene SOA are caric acid, OH-caronic acid, and caronic acid (Ma et al., 2009; Thomsen et al., 2021), while the major components from limonene SOA are limonaldehyde, keto-limonon aldehyde, limononic acid and keto-limononic acid (Pathak et al., 2012; Wang and Wang, 2021).

Water is ubiquitous in the atmosphere and can affect the formation mechanism of SOA and its

relevant physical and chemical properties (Sun et al., 2013). A number of field measurements have shown that the average molecular weight of the water/organic phase and activity coefficient of condensed organics would be changed due to the change of relative humidity (RH) (Seinfeld et al., 2001; Li et al., 2020). In addition, several laboratory studies have demonstrated that RH can influence the ozonolysis of monoterpenes in different ways. Most of those studies have reported either an inhibitory effect or a negligible effect of high RH on the particle formation (Bonn and Moortgat, 2002; Fick et al., 2002; Zhao et al., 2021; Ye et al., 2018). Nevertheless, few other studies found that high RH can promote SOA formation from the ozonolysis of limonene (Yu et al., 2011; Gong et al., 2018; Xu et al., 2021), but the reason of this promotion effect remains unclear.

To fully examine the effects of water on SOA formation from the ozonolysis of monoterpenes, especially the related chemical processes, we used an oxidation flow reactor (OFR) to investigate the ozonolysis of limonene and Δ^3-carene under different RH conditions in this study. An ultra-high performance liquid chromatography with a quadrupole time-of-flight mass spectrometer (UPLC-Q-TOF-MS) was deployed to analyze the molecular chemical composition of the SOA, which provided insights into the physical and chemical processes influenced by the water content. With these state-of-the-art techniques, we proposed mechanisms that may explain the inhibitory or enhancing RH effects on SOA formation for different monoterpenes.

2 Experimental methods

2.1 Oxidation flow reactor experiments

A series of dark ozonolysis experiments of limonene and Δ^3-carene were conducted in a custom-made oxidation flow reactor (OFR). The OFR is a 602 mm long stainless cylinder with a volume of 2.5 L (Fig. S2) (Liu et al., 2019; Liu et al., 2014). A zero-air generator (XHZ2000B, Xianhe, China) was used to generate dry clean air as the carrier gas for the OFR. As shown in Fig. S2, there are four gas paths upstream of the OFR: the first path is the precursor gas channel through which monoterpenes are injected via a syringe pump (ISPLab 01, Shenchen, China); the second path is for the flow of 300 sccm dry zero air passing through a mercury lamp ($\lambda = 185$ nm) to generate O_3; the third path is connected to a water bubbler to generate wet air; the fourth path is the extra dry zero air entering the OFR. The RH in the OFR was controlled by adjusting the ratio of the wet and dry zero air flows. A water recycle system was

equipped to keep the temperature (T) around at 298 K. The total flow was 0.9 L min^{-1}, resulting in an average residence time of 167 s. The RH and T in the OFR were monitored by a T/RH Sensor (HM40, VAISALA, Finland). The concentration of ozone and the consumption of the precursor gas were measured with an ozone monitor (Model 106L, 2B Technologies, USA) and a gas chromatography with flame ionization detector (GC-FID 7890B, Agilent Technologies, USA), respectively. The GC was equipped with a DB-624 column (30 m × 0.32 mm, 1.8 µm film thickness) whose temperature was set to ramp from 100 °C to 180 °C at a rate of 20 °C min^{-1}, and then held at 180 °C for 2 min. Before each experiment, O$_3$ was introduced into the OFR to clean it until the background aerosol mass concentration reached < 1 µg m^{-3}.

The experimental conditions are shown in Table 1. In these OFR experiments, the precursor (limonene or Δ^3-carene) concentration was set to ~320-340 ppb. A high O$_3$ concentration of ~6 ppm was used to realize an equivalent aging time of 0.41 day in the real atmosphere, assuming an average ambient O$_3$ concentration of 28 ppb (Sbai and Farida, 2019) (see Section S1 for the calculation). Under such conditions, most of the precursors were consumed, since the residence time was almost five and three times of the half-life for limonene and Δ^3-carene, respectively. Correspondingly, the O$_3$ consumption for limonene and Δ^3-carene were ~250 ppb and ~100 ppb, respectively. A series of RH conditions ranging from dry (1-2%) to 60% with a step of ~10% were used to investigate the effects of water content on SOA production and composition (see Table 1). All materials used in the experiments have been described in Section S2.

Table 1. Experimental conditions and results.

Exp.	[Precursor] (ppb)	[O]$_3$ (ppm)	T (K)	RH (%)	N$_{(13.8-723.4\ nm)}$[a] (cm^{-3})	M$_{(13.8-723.4\ nm)}$[b] (µg m^{-3})	D$_{(mean)}$[c] (nm)	SOA yield (%)
				limonene				
1	321±39	5.7	298	1–2	6.9×10^5	980.9	138.2	62.9
2	321±39	6.0	298	10±2	1.3×10^6	1377.5	126.8	88.4
3	321±39	5.9	298	20±2	9.0×10^5	1573.3	150.9	90.2
4	321±39	5.9	298	30±2	1.4×10^6	1573.3	128.9	100.9
5	321±39	6.0	298	40±2	1.7×10^6	2051.4	130. 7	131.6

4

6	321±39	5.5	298	50±2	$1.5×10^6$	1962.7	137.8	125.9
7	321±39	5.5	298	60±2	$1.5×10^6$	2211.1	139.0	141.8
Δ^3-carene								
8	341±28	6.1	298	1–2	$9.5×10^4$	346.0	195.8	19.4
9	341±28	6.4	298	10±2	$1.4×10^5$	300.3	163.4	16.8
10	341±28	6.4	298	20±2	$9.4×10^4$	244.9	176.9	13.7
11	341±28	6.0	298	30±2	$5.9×10^4$	241.2	205.1	13.5
12	341±28	6.3	298	40±2	$4.6×10^4$	205.8	203.2	11.5
13	341±28	6.3	298	50±2	$6.8×10^4$	196.7	180.7	11.0
14	341±28	6.3	298	60±2	$5.6×10^4$	198.5	190.2	11.1

[a] $N_{(14.1-735\ nm)}$ means the total particle number concentration from size 13.8 nm to 723.4 nm. [b] $M_{(13.8-723.4\ nm)}$ means the total particle mass concentration from size 13.8 nm to 723.4 nm. [c] $D_{(mean)}$ means the particle mean diameter.

2.2 SOA particle analysis

2.2.1 SOA yield

The SOA particle size distribution was measured with a scanning mobility particle sizer (SMPS), which consists of a differential mobility analyzer (DMA) (model 3082, TSI Inc., USA) and a condensation particle counter (CPC) (model 3776, TSI Inc., USA). The samples were measured by SMPS every 5 minutes with a sampling flow and a sheath flow of 0.3 L min^{-1} and 3 L min^{-1}, respectively. The SOA mass concentration was calculated from the volume concentration measured with SMPS and the aerosol density, which was estimated to be 1.25 cm^{-3} for limonene- and 1.09 g cm^{-3} for Δ^3-carene-SOA (Thomsen et al., 2021; Watne et al., 2017).

The SOA yield (Y) for individual organic gas can be calculated as:

$$Y=\frac{\Delta M}{\Delta HC}$$

Where ΔM is the total mass concentration of SOA, ΔHC is the mass concentration of reacted precursor (Ng et al., 2007; Odum et al., 1996).

2.2.2 Ultra-high performance liquid chromatography quadrupole time-of-flight mass spectrometry analysis

An ultra-high performance liquid chromatography (UPLC, UltiMate 3000, Thermo Scientific)

coupled with a quadrupole time-of-flight mass spectrometry (Q-TOFMS, Bruker Impact HD) was used to analyze the molecular-level chemical composition of SOA. First, the SOA particles were collected on the PTFE filters (47 mm diameter, 0.22 μm pore size, Jinteng, China). Next, these filters were dissolved and extracted by 5 mL methanol for two times. Extracts were then filtered through PTFE syringe filters (0.22 μm pore size), and were concentrated to near dryness by nitrogen-blowing. At last, the samples were redissolved in a 200 μL solution with 0.1% (v/v) formic acid in 50:50 methanol/ultrapure water mixture.

The parameters of LC-MS were set as follows: capillary voltage 4000 V, nebulizer pressure 0.4 bar, dry heater temperature 200℃, end plate voltage −500 V, and flow of dry gas 4 L min^{-1}. A C_{18} column (100 Å, 3 mm particle size, 2.1 mm×50 mm, Waters, USA) was used with a column temperature of 35℃. The mobile phase was 0.1 % formic acid in methanol (A) and 0.1 % formic acid in ultra-high purity water (B) with a flow of 200 μL min^{-1}. The injection volume was 5 μL. The MS was operated in negative ion mode, and the detection molecular weight range was from m/z 50 to 1500. The temperature ramp program was: 0–3min with 0%–3% phase B, 3–25min with 3%–50% phase B, 25–43min with 50%–90% phase B, 43–48 min with 90%–3% phase B, 48–60min with 3% phase B.

3 Results and discussion

3.1 SOA production under different RH conditions

SOA formation of a representative experiment is shown in Fig. S3. It is found that the formed SOA are mainly in the size range of 60-200 nm, and the number concentration and mass concentration are relatively stable during the course of the OFR experiment. SOA formation from limonene and Δ^3-carene in terms of particle number concentration, particle mass concentration, and SOA yield as a function of RH are illustrated in Fig. 1a-c. We find that all the above-mentioned 3 parameters of limonene-SOA increase with the increasing RH. The increment of particle mass concentration and SOA yield from the ozonolysis of limonene is ~100% higher at wet (60% RH) than at dry conditions. In contrast, SOA formation from Δ^3-carene is suppressed by ~40% under high RH. The distinct effects of RH on SOA formation from the ozonolysis of limonene and Δ^3-carene found in this study agree with most previous studies (Yu et al., 2011; Jonsson et al., 2006b; Bonn et al., 2002; Gong and Chen, 2021; Li et al., 2019b). As shown in Table 2, Yu et al. (2011) reported a positive correlation between SOA production and RH

for the ozonolysis of limonene in the chamber experiments without OH scavenger. Their experimental condition is similar to that in our study regarding the absence of OH scavenger and, thus, similar results were observed. However, in the presence of OH scavenger, results are quite different. Jonsson et al. (2006) observed a similar enhancement effect of high RH on SOA production with 2-butanol as the OH scavenger, while Bonn et al. (2002) found a negligible or suppressive effect with cyclohexane as the OH scavenger. It should be noted that the OH scavenger not only has the ability to scavenge OH but also produces additional products which may influence the reactions of target precursors. For example, there is no difference between 2-butanol and cyclohexane in the scavenging ability of OH radical, though 2-butanol will produce more $HO_2\cdot$ than cyclohexane and, consequently, $R\cdot$ will react with $HO_2\cdot$ to produce more hydroxyl acids and hydroxyl per-acid products, most of which have low volatility and, thus high partitioning into the particle phase. According to previous studies, the influence of different OH scavengers can vary (Jonsson et al., 2008). This may explain the different findings with and without OH scavenger for limonene-SOA. With regard to Δ^3-carene, similar results are found in the absence of OH scavenger, namely, high RH has negligible or slightly suppressive effect on SOA production (Bonn et al., 2002; Fick et al., 2002). Same as limonene, the presence of OH scavenger and its different chemical nature can explain the different results found previously (Jonsson et al., 2006a; Bonn et al., 2002).

The enhancement in limonene-SOA production under high RH can be due to several reasons from either physical or chemical processes. First, the hygroscopic growth of the particles (i.e., absorption of water content) can lead to higher mass concentration under higher RH, but the enhancement should be at most ~30% as the growth factor (GF, the ratio of wet and dry diameter: $D_{wet/Ddry}$) of limonene-SOA is ≤1.1 (Varutbangkul et al., 2006). However, we do not observe an obvious change in the mean diameter when comparing dry and wet conditions (Fig. 1d). In addition, hygroscopic growth should also occur for Δ^3-carene SOA, but no obvious enhancement in particle mass is observed (Fig. 1a). Therefore, it is suggested that physical processes regarding hygroscopic growth play a minor role in the enhancement in limonene-SOA under high RH. As a consequence, we believe that chemical processes are likely the reason of the enhancement in limonene-SOA under high RH. Water can influence chemical processes in the gas phase or in the particle phase. Particle-phase reactions can promote the growth of small particles and, thus, mainly lead to larger particle sizes. As the observed SOA enhancement is mainly from high number concentration particles rather than the large size particles (Fig. 1b and 1d), it is likely that the

184   water-participated gas-phase reactions are the most possible reasons for the limonene-SOA enhancement.

185   The reaction mechanism is analyzed below based on the mass spectra information on the SOA.
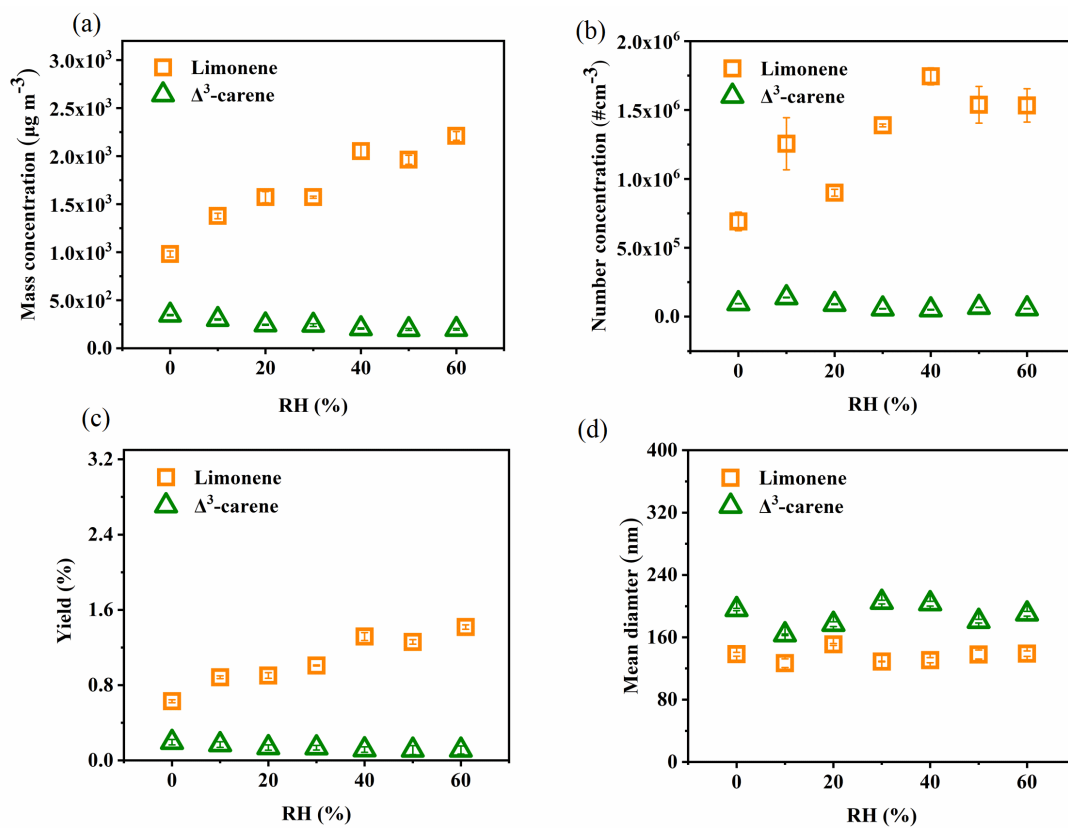
186

187   **Figure 1.** The effect of RH on the SOA formation: (a) number concentration, (b) mass concentration, (c)

188   SOA yield, (d) mean diameter.

189

190

Table 2. Comparison with previous studies on the effect of RH.

Precursor	Precursor concentration (ppb)	O₃ concentration (ppb)	Reactor	OH scavenger	T (K)	RH (%)	SOA Mass Concentration (μg/m³)	SOA Yield (%)	Mᵃ	Nᵇ	Reference
limonene	1000	1000	flow reactor	cyclohexane	295±2	0.02 and 32.5	N.Mᶜ	N.Mᶜ	no effect	–ᵉ	Bonn et al. (2002)
	320	100±5	chamber	N.Mᶜ	296±2	18±2, 50±3 and 82±2	24; 58; 120	7.0 ± 0.7; 17.4±1.3; 53.4±1.9	+ᵈ (7 times)	+ᵈ (8 times)	Yu et al. (2011)
	15 and 30	430.9	flow reactor	2-butanol	298±0.4	< 2-85	2.7-10.5 and 62-229	6.8-26.4 and 77.4-285.7	+ᵈ	+ᵈ	Jonsson et al. (2006)
	endocyclic (24.6) and exocyclic (15.2)	endocyclic (270) and exocyclic (12200)	flow reactor	2-butanol	298	10-50	endocyclic (~11) and exocyclic (22-51)	endocyclic (~7.4) and exocyclic (23.8-55.3)	exocyclic (+ᵈ) and endocyclic (–ᶜ)	N.Mᶜ	Gong and Chen (2021)
	1085	900±10	flow reactor	none	298	3-62	150; 200; 210	N.M	+ᵈ	–ᵉ	Li et al. (2019)

	321±39	5786±203	flow reactor	none	298	0-60	980.9-2211.1	62.9-141.8	+[d] (2 times)	+[d] (3 times)	this study
	1000	1000	flow reactor	cyclohexane	295±2	0.02 and 32.5	N.M[c]	N.M[c]	no effect	−[e]	Bonn et al. (2002)
	14.2 and 29.4	2300	flow reactor	2-butanol	298±0.4	<2-85	0.78-3.8 and 15.3-94;	2.1-10.1and 19.8- 116.7	+[d]	+[d]	Jonsson et al. (2006)
Δ^3-carene	1111	900±10	flow reactor	none	298	3-62	75; 80; 90	N.M	−[e]	−[e]	Li et al. (2019)
	341±28	6257±140	flow reactor	none	298	0-60	346.0-198.5	19.4-11.1	−[e]	no effect	this study

191   [a] M means the change trend total particle mass concentration. [b] N means total particle number concentration. [c] N.M. means not mentioned. [d] Positive sign (+) means the

192   mass or number concentration increases with RH. [e] Negative sign (−) means the mass or number concentration decreases with RH.

3.2 Molecular analysis of SOA particles

The UPLC/ESI-Q-TOF-MS was used to examine the SOA molecular composition under high and low RH conditions. As shown in Fig. 2a, the mass spectra of limonene-SOA are divided into four groups: monomeric group (<m/z 300), dimeric group (m/z 300-500), trimeric group (m/z 500-700), and tetrameric group (m/z 700-1000), corresponding to products containing one, two, three, and four oxygenated limonene units, respectively (Bateman et al., 2009). Most of the SOA molecules are monomers (>60%) (Fig. 2b) and dimers (~25%), while trimers and tetramers contribute to very small fractions (<10% and ~3%) (Table S1). Correspondingly, the distribution of Δ^3-carene-SOA can be divided into four groups (Fig. S4), comparable to that of limonene-SOA. Most of the SOA molecules are monomers (~70%) and dimers (~25%), while trimers and tetramers contribute to smaller proportions (~2% and <1%, respectively) (Table S2). Although the SOA mass concentration increases by ~100% under high RH condition, the relative intensities of MS peaks do not significantly change with varying RH conditions. In other words, we did not observe an obvious change in the overall MS patterns, and the fractions of the four groups only slightly differed under different RH conditions, e.g., the fraction of monomers was 62% under dry condition and 66% under wet conditions. However, if we take a closer look, the intensities and contributions of specific peaks are quite different with varying RH. For example, the relative intensity of $C_{10}H_{16}O_2$, a possible first-generation product (Gong et al., 2018), decreases by ~20% with increasing RH from dry to 60% (Table S3). This is likely due to the multi-generation reactions influenced by water vapor concentration, as discussed below with the proposed reaction mechanism of limonene ozonolysis.
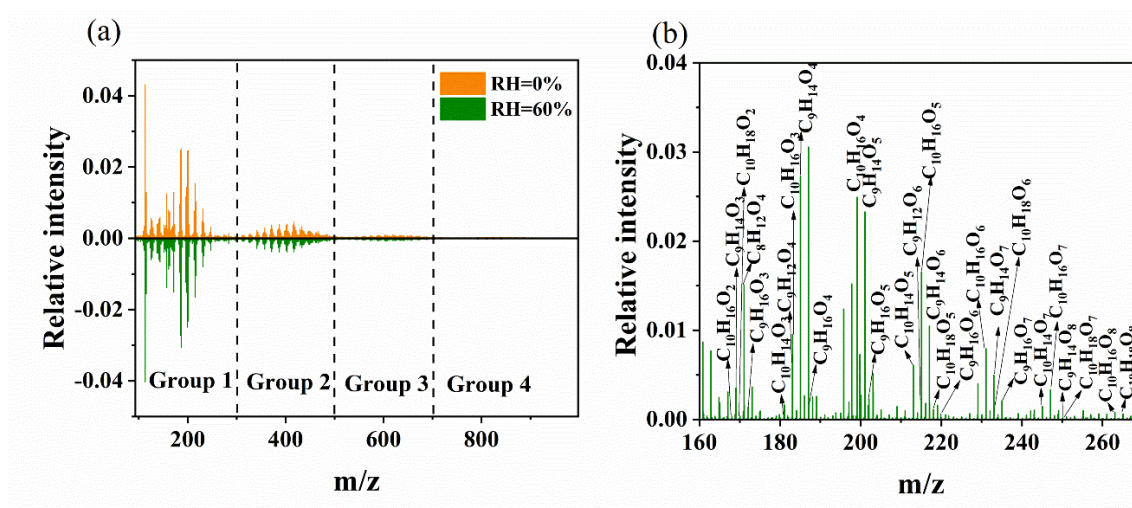
Figure 2. UPLC/ (−) ESI-Q-TOF-MS mass spectra of SOA from limonene ozonolysis. (a) MS under high and low RH conditions; (b) the identification of monomers under high RH condition.

The proposed reaction mechanism of limonene ozonolysis is shown in Fig. 3 and Fig. 4. The initial step in the reaction of O_3 with limonene is the attack of the endocyclic double bond to form eCI_1 and eCI_2 (with branching ratios of 0.35 and 0.65, respectively). In the context of eCI_1, several complex reactions occur, with the most dominant reaction being the generation of hydroxyl radicals (OH) and a reaction pathway known as sCI_1. The sCI_1 pathway can proceed through three distinct reactions, as depicted in Fig. 3. The first pathway is the reaction with H_2O, alcohol or carboxylic acid to form a carboxylic acid species with hydroxyl, which would subsequently lose a molecule of water to form limononaldehyde or lose a molecule of hydrogen peroxide to form limononic acid (Grosjean et al., 1992; Li et al., 2019b). The second and third pathways involve reactions of sCI_1 with carboxylic acids and carbonyls, respectively, leading to the formation of anhydrides and secondary ozonides. Additionally, the generated OH radicals can react with limonene, giving rise to another alkyl radical, $C_{10}H_{17}O\cdot$. These alkyl radicals react with O_2 and form peroxy radicals ($RO_2\cdot$). The atmospheric fate of produced $RO_2\cdot$ in the absence of NO_x includes the reaction with $RO_2\cdot$ or $HO_2\cdot$ (Atkinson and Arey, 2003) and the unimolecular H shift. The $RO_2\cdot + HO_2\cdot$ route mainly form hydroperoxide (ROOH), and the minor fraction is to form alcohols and carbonyls (Atkinson and Arey, 2003). The products of bimolecular reactions between $RO_2\cdot$ and $RO_2\cdot$ are alcohols, carbonyls, alkoxy radicals, peroxides and ROOR dimers (Hammes et al., 2019; Peng et al., 2019). The H shift of $RO_2\cdot$ can form second-generation $R\cdot$ and trigger a main generation channel of highly oxidized molecules (HOMs), i.e., $R\cdot$ would go through a process of repeated oxygen addition and hydrogen-atom shift to form HOMs with high O/C ratios of > 0.7–0.8 (Molteni et al., 2018; Bianchi et al., 2019).

In addition to the eCI_1 route, the eCI_2 pathway is also responsible for the generation of various products (Fig. 4). Since the reaction of the hydroxyl radical (OH) attacking limonene is already depicted in Fig. 3, our main emphasis in Fig. 4 is on the pathways involved in the generation of SCI. First, sCI_2 reacts with H_2O and decomposes to limononaldehyde and H_2O_2. Additionally, sCI_2 could experience an O_2 addition, $\cdot$OH loss and isomerization to produce two types of $RO_2\cdot$, which can undergo the similar reactions as the $RO_2\cdot$ formed from the sCI_1 route, and the major products are also shown in Fig. 4.

Since limonene and Δ^3-carene both have an endocyclic double bond, the similar reactions as

12

243 mentioned above can occur for the ozonolysis of Δ^3-carene (Fig. S5), and most corresponding formula

244 in Fig. S5 could be identified in Table S4. However, the reactivity of limonene towards O_3 is expected to

245 be higher owing to its exocyclic double bond. As shown in Fig. 4, the attack of O_3 to the exocyclic double

246 bond mainly leads to sCI_3 (highlighted in red) with the unpaired electrons outside the ring (Leungsakul

247 et al., 2005). sCI_3 can react with H_2O to form a carbonyl called keto-limonene. It should be noted that

248 this reaction can occur not only for limonene, but also for all the products that retain the exocyclic double

249 bond. As a result, the compounds that are colored in blue in Fig. 3 and Fig. 4 can undergo further reactions

250 to generate products with an additional carbonyl (see the boxes in Fig. 3 and Fig. 4). Furthermore, their

251 molecular formula shown in Table S5 have been identified using the Q-TOF-MS. This mechanism can

252 well explain the decrease in the relative intensity of $C_{10}H_{16}O_2$ from high RH to low RH and the increase

253 in the relative intensity of $C_9H_{14}O_3$ from low RH to high RH (Table S3).

254 In such progress, we cannot rule out the possibility that relative humidity (RH) may influence the

255 generation of other free radicals (Ma et al., 2009), thereby impacting the formation of secondary organic

256 aerosols (SOA), such as, OH-radical reactions (Bonn et al., 2002; Fick et al., 2002). However, Molar OH

257 radical yields were reported as 0.65±0.10 (Hantschke et al., 2021), 0.86±0.11 (Aschmann et al., 2002)

258 and 0.56 to 0.59 (Wang et al., 2019) for Δ^3-carene, while for limonene, the reported yields were 0.67±0.10

259 (Aschmann et al., 2002) and 0.76±0.06 (Herrmann et al., 2010). It seems that the OH radicals produced

260 from limonene and Δ^3-carene are quite similar within the range of uncertainties. Therefore, the increased

261 ozone consumption by limonene is primarily attributed to the presence of its exocyclic double bond.

262
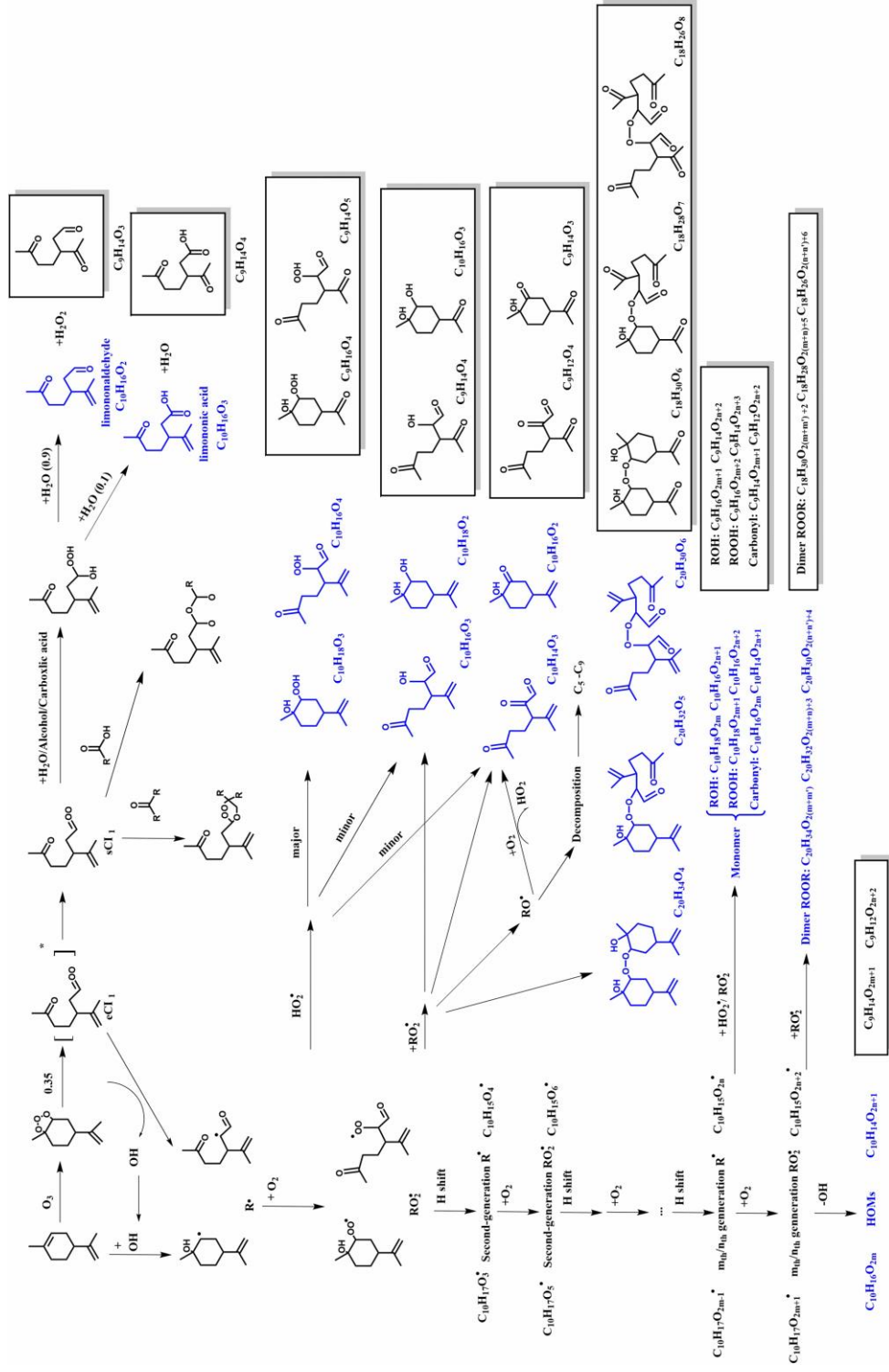
Figure 3. Proposed formation mechanism for SOA formation from eCI oxidation under high RH. The compounds in blue and in boxes are identified using UPLC/ (−) ESI-Q-

263

264   TOF-MS.

14
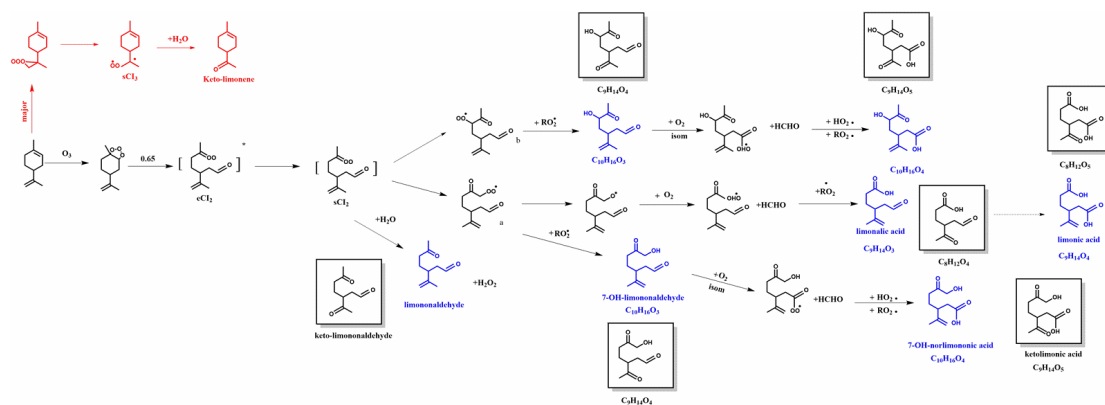
Figure 4. Proposed formation mechanisms for SOA formation from eCI_2 and exocyclic double bond oxidation under high RH. The compounds in blue and in boxes are identified using UPLC/ (−) ESI-Q-TOF-MS.

3.3 Processes leading to the increase or decrease in SOA formation

Based on the results and mechanisms shown above, we present evidence that high humidity enhances limonene-SOA formation. First, the presence of water vapor enhances the formation of carbonyls from the reaction of exocyclic double bond, and the oligomerization of these carbonyls generates more dimers including hemiacetal (or acetal) formation and aldol condensation (Zhang et al., 2022; Kroll et al., 2005; Jang et al., 2003). As shown in Table S6, 54 out of the total 187 dimers were exclusively observed for limonene under high humidity conditions, contributing to a corresponding intensity of ~19%. These dimers can be classified as low-volatile organic compounds (LVOC; $3\times10^{-4} < C_0 < 0.3$ μg m^{-3}) and extremely low-volatile organic compounds (ELVOCs; $C_0 < 3\times10^{-4}$ μg m^{-3}) (Fig. 5a), and thus promote the nucleation and new particle formation in different ways. This finding is similar to that from a previous study showing that high RH can promote dimer formation from the ozonolysis of α-pinene (Kristensen et al., 2014). Second, we find that high RH can also promote the formation of HOMs, although the mechanism remains unclear. As shown in Table S3, many HOMs proposed from the mechanism are detected under high RH condition but not detected under low RH condition, including both monomers and dimers. Many HOMs have low volatilities and, thus, can also promote new particle formation. Overall, the promoted dimer and HOM formation greatly enhance the new particle number concentration under high RH condition (Fig. 6).

15
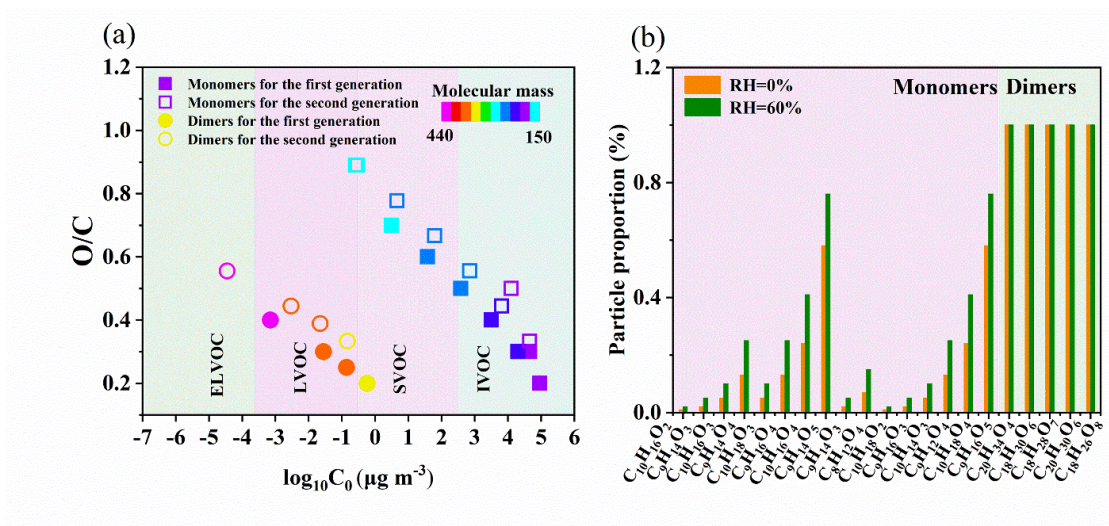
Figure 5. (a) Distribution of the limonene-SOA in the two-dimensional volatility basis set (2D-VBS) space. (b) Partitioning coefficients of limonene monomers and dimers under low and high RH conditions.
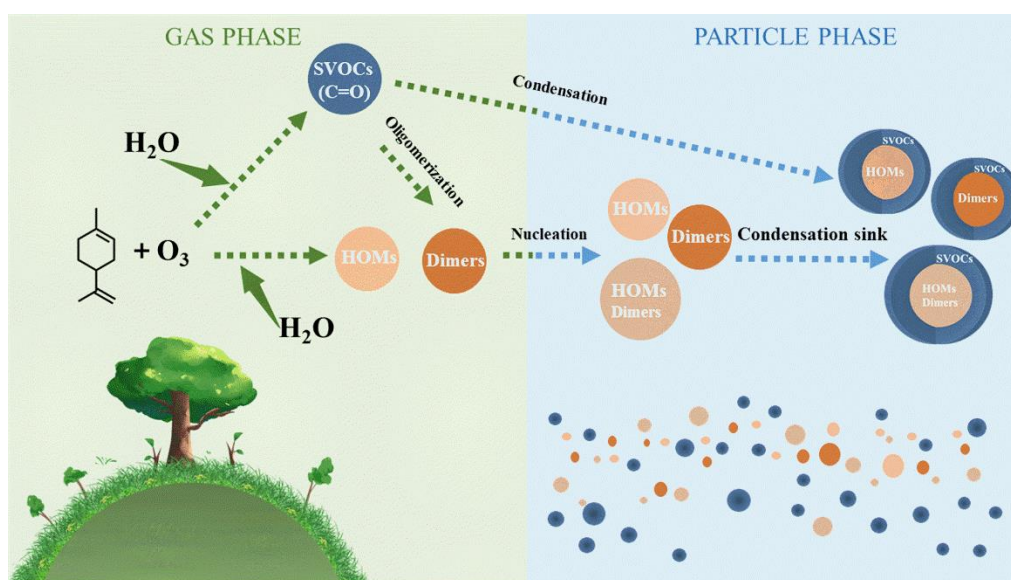
Figure 6. Schematic diagram of the possible mechanisms for the enhancement of limonene-SOA.

High particle number concentration generally provides more surface areas for semi-volatile organic compounds (SVOCs; $0.3 < C_0 < 300$ µg m^{-3}) to condense on, which results in higher condensation sink (CS). In the OFR, the fates of SVOCs include condensing on aerosol, getting lost on the wall, and reacting with OH radicals to form functionalization and/or fragmentation products (Palm et al., 2016; Li et al., 2019a). The promoted condensation by higher CS leads to a higher fraction of SVOCs getting into the particle phase rather than getting lost on the wall or becoming smaller fragments staying in the gas phase,

and thus promoting SOA formation (Li et al., 2019a). Furthermore, the transformation from C-C double bond to carbonyl shown in Fig. 3 and Fig. 4 decreases the volatility of molecules, which can largely influence the gas-particle partitioning of the monomeric compounds (Fig. 5b). For example, the C_0 values of $C_{10}H_{16}O_2$ and $C_{10}H_{16}O_3$ are 90701 and 19968 μg m^{-3}, corresponding to partitioning coefficients of 0.01 and 0.05, respectively (Fig. 5b and Table S3), with an SOA mass concentration of ~1000 μg m^{-3} under dry condition. When they are converted to carbonyls $C_9H_{14}O_3$ and $C_9H_{14}O_4$, the values of C_0 become 45556 and 6479 μg m^{-3}, corresponding to partitioning coefficients of 0.02 and 0.13, respectively (Fig. 5b and Table S3), with the same SOA loading. This enhancement in partitioning coefficient can largely promote the condensation of SVOCs and, thus, enhance the SOA mass concentration. In addition, the enhanced SOA formation can further influence the equilibrium, e.g., the partitioning coefficient of $C_{10}H_{16}O_3$ increases from 0.05 to 0.10 when SOA mass concentration increases from ~1000 μg m^{-3} under dry condition to ~2000 μg m^{-3} under wet condition (Fig. 5b and Table S3). The distribution of saturation vapor pressure for monomers and dimers identified by MS has also been shown in Fig. 5a. As can be seen from this figure, around 50% monomers are categorized as SVOCs, thus having the large fraction in the particle phase when converting from dry to wet conditions. Overall, the different fate and partitioning of SVOCs largely enhance the amount of SVOCs in the particle phase (Fig. 6).

Concluding the analysis above, high humidity promotes the SOA formation from the ozonolysis of limonene in two steps: nucleation of new particles and condensation of SVOCs on them (Fig. 6). These two steps are closely related to the multi-generation reactions of the exocyclic C=C bond, which are unlikely to happen for the ozonolysis of Δ^3-carene. Interestingly, Gong and Chen (2021) have found that high RH can inhibit the SOA formation from the first-generation oxidation of limonene ozonolysis, but enhance the SOA formation from the second-generation oxidation (Gong and Chen, 2021), their results agree well with the results and analysis shown here. In contrast, Li et al. (2019b) found negligible change in dimers and HOMs in limonene-O_3 system when changing RH from 0 to 60%. The discrepancy is mainly attributed to the different experimental conditions. The ozone exposure in this study is ~18 times higher than in Li et al. (2019b), while the limonene concentration in this study is only ~30% of that in their study. These two conditions both favor the multi-generation reactions occurred at the exocyclic double bond of limonene and its products. Thus, we believe this leads to the different results regarding the formation of HOMs and dimers.

329 Regarding Δ^3-carene, the mechanisms and processes are almost opposite to those of limonene. First,

330 water vapor reacts with sCI_1 or sCI_2 to promote the formation of α-hydroxyalkyl-hydroperoxides (Fig.

331 S5). Their subsequent products without second ozonolysis of exocyclic double bond have higher

332 volatility, and may most likely prevail in the gas phase. In addition, it has been found that α-hydroxyalkyl

333 hydroperoxides preferentially decompose into aldehydes and H_2O_2 (Kumar et al., 2014; Chen et al., 2016),

334 i.e., 3-caronaldehyde for Δ^3-carene, which has higher volatility than the products from other reaction

335 pathways. Correspondingly, the number and relative intensity of HOMs and dimers detected under high

336 RH conditions are both lower than those under low RH conditions (Table S7). Furthermore, out of a total

337 of 178 dimers, 63 dimers were exclusively identified under low RH conditions (Table S6). As a result,

338 high RH shows an inhibitory effect on the SOA formation from Δ^3-carene ozonolysis.

339 To investigate the multi-generation reactions of limonene under low-concentration conditions, we

340 conducted low-concentration limonene ozonolysis experiments, and the results are shown in Fig. S6. In

341 these experiments, the limonene and O_3 concentrations were 20.5 ppb and 5.7 ppm, respectively.

342 According to the experimental results, the number concentration of SOA formed from limonene

343 ozonolysis increased by approximately 1.4 times under high RH, which is similar to the increase observed

344 under high-loading conditions. The mass concentration increased by approximately 1.3 times at a

345 precursor concentration of 20.5 ppb. The relatively small increase in mass concentration compared to the

346 high-concentration conditions may be attributed to the less pronounced distribution of SVOCs at low

347 mass concentrations. This result indicates that the enhancement effect on limonene SOA by high RH is

348 still valid for low precursor concentrations.

349 To further confirm the assumption that water-influenced multi-generation reactions of the exocyclic

350 double bond enhance the SOA formation, we conducted two comparative analyses: firstly, we examined

351 the ozonolysis of the endocyclic double bond in limonene, leaving the exocyclic double bond unreacted.

352 This was done by applying a low O_3 concentration (~67 ppb), since the reaction of O_3 with endocyclic

353 double bond is ~30 times faster than the reaction of O_3 with exocyclic double bond (Shu and Atkinson,

354 1994). Interestingly, when limonene was oxidized at only the endocyclic double bond, we observed a

355 slight decrease in both the number and mass concentrations as the RH increased (Fig. S7). This is similar

356 to the results obtained for Δ^3-carene, which contains only one endocyclic double bond. Secondly, we

357 compared the ozonolysis of structurally similar β-caryophyllene, which has an exocyclic C-C double

bond that can undergo further reactions (Fig. S8). As expected, we observe a large enhancement in SOA formation under high RH condition (Table S8 and Fig. S9). This implies that monoterpenes, sesquiterpenes, and other BVOCs with two unsaturation double bonds may follow similar reaction mechanisms during ozonolysis, and thus have a RH dependency in SOA production.

4 Conclusions

In this study, the effect of humidity on SOA production from the ozonolysis of two monoterpenes (limonene and Δ^3-carene) was investigated with an OFR. Contrasting impacts of RH on the SOA formation were observed: limonene-SOA yield increases by ~100% when RH changes from ~1% to ~60%, while Δ^3-carene-SOA yield slightly decreases. By analyzing the chemical composition of SOA with ESI-Q-TOF-MS, we find that the multi-generation reactions of the exocyclic C-C double bond are likely the driving force of the enhancement in limonene-SOA. The presence of water promotes the formation of carbonyls from the reaction of exocyclic double bond, and further favors the formation of dimers and HOMs. This leads to promoted new particle formation and subsequent condensation of SVOCs. These reactions also lower the volatilities of the SVOCs, and further promote the gas-particle partitioning. Moreover, this hypothesis is proved by a similar behavior of the ozonolysis of β-caryophyllene (sesquiterpene with an exocyclic double bond) in SOA enhancement under high RH condition. The results in this study suggest that multi-generation reactions play an important role in SOA formation from the ozonolysis of BVOCs, which are significantly influenced by humidity. This impact is largely dependent on the molecular structure of the SOA precursors (e.g., with or without the exocyclic double bond), thus highlighting the importance to consider the molecular structure of monoterpenes in modeling and field studies of biogenic SOA.

Data availability. Experimental data are available upon request to the corresponding authors.

Supplement. The supplement related to this article is available online.

Author contributions. LD and SZ designed the experiments and SZ carried them out. SZ performed data analysis with assistance from KL, LD, ZY, and JL. SZ and KL wrote the paper with contributions from all co-authors.

Declaration. The authors declare that they have no conflict of interest.

Reference

Ahmadov, R., McKeen, S. A., Robinson, A. L., Bahreini, R., Middlebrook, A. M., de Gouw, J. A., Meagher, J., Hsie, E. Y., Edgerton, E., Shaw, S., and Trainer, M.: A volatility basis set model for summertime secondary organic aerosols over the eastern United States in 2006, J. Geophys. Res.-Atmos., 117, D6301, https://doi.org/10.1029/2011JD016831, 2012.

Aschmann, S. M., Arey, J., and Atkinson, R.: OH radical formation from the gas-phase reactions of O_3 with a series of terpenes, Atmos. Environ., 36, 4347-4355, https://doi.org/10.1016/S1352-2310(02)00355-2, 2002.

Atkinson, R.: Kinetics and mechanisms of the gas-phase reactions of the NO_3 radical with organic compounds, J. Phys. Chem. Ref. Data, 20, 459-507, https://doi.org/10.1063/1.555887, 1991.

Atkinson, R. and Arey, J.: Gas-phase tropospheric chemistry of biogenic volatile organic compounds: a review, Atmos. Environ., 37, 197-219, https://doi.org/10.1016/S1352-2310(03)00391-1, 2003.

Bäck, J., Aalto, J., Henriksson, M., Hakola, H., He, Q., and Boy, M.: Chemodiversity of a Scots pine stand and implications for terpene air concentrations, Biogeosciences, 9, 689-702, https://doi.org/10.5194/bg-9-689-2012, 2012.

Bateman, A. P., Nizkorodov, S. A., Laskin, J., and Laskin, A.: Time-resolved molecular characterization of limonene/ozone aerosol using high-resolution electrospray ionization mass spectrometry, Phys. Chem. Chem. Phys., 11, 7931-7942, https://doi.org/10.1039/b905288g, 2009.

Bianchi, F., Kurtén, T., Riva, M., Mohr, C., Rissanen, M. P., Roldin, P., Berndt, T., Crounse, J. D., Wennberg, P. O., Mentel, T. F., Wildt, J., Junninen, H., Jokinen, T., Kulmala, M., Worsnop, D. R., Thornton, J. A., Donahue, N., Kjaergaard, H. G., and Ehn, M.: Highly oxygenated organic molecules (HOM) from gas-phase autoxidation involving peroxy radicals: a key contributor to atmospheric aerosol, Chem. Rev., 119, 3472-3509, https://doi.org/10.1021/acs.chemrev.8b00395, 2019.

414 Bonn, B. and Moortgat, G. K.: New particle formation during α- and β-pinene oxidation by O_3, OH and

415 NO_3, and the influence of water vapour: particle size distribution studies, Atmos. Chem. Phys., 2, 183-

416 196, https://doi.org/10.5194/acp-2-183-2002, 2002.

417 Bonn, B., Schuster, G., and Moortgat, G. K.: Influence of water vapor on the process of new particle

418 formation during monoterpene ozonolysis, J. Phys. Chem. A, 106, 2869-2881,

419 https://doi.org/10.1021/jp012713p, 2002.

420 Chen, H., Ren, Y., Cazaunau, M., Dalele, V., Hu, Y., Chen, J., and Mellouki, A.: Rate coefficients for the

421 reaction of ozone with 2-and 3-carene, Chem. Phys. Lett., 621, 71-77,

422 https://doi.org/10.1016/j.cplett.2014.12.056, 2015.

423 Chen, L., Huang, Y., Xue, Y., Shen, Z., Cao, J., and Wang, W.: Mechanistic and kinetics investigations

424 of oligomer formation from Criegee intermediate reactions with hydroxyalkyl hydroperoxides, Atmos.

425 Chem. Phys., 19, 4075-4091, https://doi.org/10.5194/acp-19-4075-2019, 2019.

426 Chen, L., Wang, W., Wang, W., Liu, Y., Liu, F., Liu, N., and Wang, B.: Water-catalyzed decomposition

427 of the simplest Criegee intermediate CH_2OO, Theor. Chem. Acc., 135, 131,

428 https://doi.org/10.1007/s00214-016-1894-9, 2016.

429 Chen, X. and Hopke, P. K.: A chamber study of secondary organic aerosol formation by limonene

430 ozonolysis, Indoor Air, 20, 320-328, https://doi.org/10.1111/j.1600-0668.2010.00656.x, 2010.

431 Cholakian, A., Beekmann, M., Coll, I., Ciarelli, G., and Colette, A.: Biogenic secondary organic aerosol

432 sensitivity to organic aerosol simulation schemes in climate projections, Atmos. Chem. Phys., 19, 13209-

433 13226, https://doi.org/10.5194/acp-19-13209-2019, 2019.

434 de Matos, S. P., Teixeira, H. F., de Lima, Á. A. N., Veiga-Junior, V. F., and Koester, L. S.: Essential oils

435 and isolated terpenes in nanosystems designed for topical administration: a review, Biomolecules, 9, 138,

436 https://doi.org/doi:10.3390/biom9040138, 2019.

437 Drozd, G. T. and Donahue, N. M.: Pressure dependence of stabilized Criegee intermediate formation

438 from a sequence of alkenes, J. Phys. Chem. A, 115, 4381-4387, https://doi.org/10.1021/jp2001089, 2011.

439 Fick, J., Pommer, L., Andersson, B., and Nilsson, C.: A study of the gas-phase ozonolysis of terpenes:

440 the impact of radicals formed during the reaction, Atmos. Environ., 36, 3299-3308,

441 https://doi.org/10.1016/s1352-2310(02)00291-1, 2002.

442 Gong, Y. and Chen, Z.: Quantification of the role of stabilized Criegee intermediates in the formation of

443   aerosols in limonene ozonolysis, Atmos. Chem. Phys., 21, 813-829, https://doi.org/10.5194/acp-21-813-

444   2021, 2021.

445   Gong, Y., Chen, Z., and Li, H.: The oxidation regime and SOA composition in limonene ozonolysis: roles

446   of different double bonds, radicals, and water, Atmos. Chem. Phys., 18, 15105-15123,

447   https://doi.org/10.5194/acp-18-15105-2018, 2018.

448   Grosjean, D., Williams, E. L., and Seinfeld, J. H.: Atmospheric oxidation of selected terpenes and related

449   carbonyls: gas-phase carbonyl products, Environ. Sci. Technol., 26, 1526-1533,

450   https://doi.org/10.1021/es00032a005, 1992.

451   Guenther, A. B., Jiang, X., Heald, C. L., Sakulyanontvittaya, T., Duhl, T., Emmons, L. K., and Wang, X.:

452   The model of emissions of gases and aerosols from nature version 2.1 (MEGAN2.1): an extended and

453   updated framework for modeling biogenic emissions, Geosci. Model Dev., 5, 1471-1492,

454   https://doi.org/10.5194/gmd-5-1471-2012, 2012.

455   Guo, S., Hu, M., Zamora, M. L., Peng, J., Shang, D., Zheng, J., Du, Z., Wu, Z., Shao, M., Zeng, L.,

456   Molina, M. J., and Zhang, R.: Elucidating severe urban haze formation in China, Proc. Natl. Acad. Sci.

457   U. S. A., 111, 17373-17378, https://doi.org/10.1073/pnas.1419604111, 2014.

458   Hammes, J., Lutz, A., Mentel, T., Faxon, C., and Hallquist, M.: Carboxylic acids from limonene oxidation

459   by ozone and hydroxyl radicals: insights into mechanisms derived using a FIGAERO-CIMS, Atmos.

460   Chem. Phys., 19, 13037-13052, https://doi.org/10.5194/acp-19-13037-2019, 2019.

461   Hantschke, L., Novelli, A., Bohn, B., Cho, C., Reimer, D., Rohrer, F., Tillmann, R., Glowania, M.,

462   Hofzumahaus, A., Kiendler-Scharr, A., Wahner, A., and Fuchs, H.: Atmospheric photooxidation and

463   ozonolysis of Δ3-carene and 3-caronaldehyde: rate constants and product yields, Atmos. Chem. Phys.,

464   21, 12665-12685, 10.5194/acp-21-12665-2021, 2021.

465   Herrmann, F., Winterhalter, R., Moortgat, G. K., and Williams, J.: Hydroxyl radical (OH) yields from the

466   ozonolysis of both double bonds for five monoterpenes, Atmos. Environ., 44, 3458-3464,

467   https://doi.org/10.1016/j.atmosenv.2010.05.011, 2010.

468   Huang, X., Yun, H., Gong, Z., Li, X., He, L., Zhang, Y., and Hu, M.: Source apportionment and secondary

469   organic aerosol estimation of PM2.5 in an urban atmosphere in China, Sci. China-Earth Sci., 57, 1352-

470   1362, https://doi.org/10.1007/s11430-013-4686-2, 2014.

471   Jang, M. S., Carroll, B., Chandramouli, B., and Kamens, R. M.: Particle growth by acid-catalyzed

472   heterogeneous reactions of organic carbonyls on preexisting aerosols, Environ. Sci. Technol., 37, 3828-

473   3837, 10.1021/es021005u, 2003.

474   Jokinen, T., Berndt, T., Makkonen, R., Kerminen, V.-M., Junninen, H., Paasonen, P., Stratmann, F.,

475   Herrmann, H., Guenther, A. B., Worsnop, D. R., Kulmala, M., Ehn, M., and Sipilä, M.: Production of

476   extremely low volatile organic compounds from biogenic emissions: Measured yields and atmospheric

477   implications, Proc. Natl. Acad. Sci. U. S. A., 112, 7123-7128,

478   https://doi.org/doi:10.1073/pnas.1423977112, 2015.

479   Jonsson, A. M., Hallquist, M., and Ljungstrom, E.: Impact of humidity on the ozone initiated oxidation

480   of limonene, Δ^3-carene, and α-pinene, Environ. Sci. Technol., 40, 188-194,

481   https://doi.org/10.1021/es051163w, 2006a.

482   Jonsson, A. M., Hallquist, M., and Ljungstrom, E.: Impact of humidity on the ozone initiated oxidation

483   of limonene, Delta(3)-carene, and alpha-pinene, Environ. Sci. Technol., 40, 188-194,

484   https://doi.org/10.1021/es051163w, 2006b.

485   Jonsson, A. M., Hallquist, M., and Ljungstrom, E.: Influence of OH scavenger on the water effect on

486   secondary organic aerosol formation from ozonolysis of limonene, Δ^3-carene, and α-pinene, Environ. Sci.

487   Technol., 42, 5938-5944, https://doi.org/10.1021/es702508y, 2008.

488   Kanakidou, M., Seinfeld, J. H., Pandis, S. N., Barnes, I., Dentener, F. J., Facchini, M. C., Van Dingenen,

489   R., Ervens, B., Nenes, A., Nielsen, C. J., Swietlicki, E., Putaud, J. P., Balkanski, Y., Fuzzi, S., Horth, J.,

490   Moortgat, G. K., Winterhalter, R., Myhre, C. E. L., Tsigaridis, K., Vignati, E., Stephanou, E. G., and

491   Wilson, J.: Organic aerosol and global climate modelling: a review, Atmos. Chem. Phys., 5, 1053-1123,

492   https://doi.org/10.5194/acp-5-1053-2005, 2005.

493   Khamaganov, V. G. and Hites, R. A.: Rate constants for the gas-phase reactions of ozone with isoprene,

494   α- and β-pinene, and limonene as a function of temperature, J. Phys. Chem. A, 105, 815-822,

495   https://doi.org/10.1021/jp002730z, 2001.

496   Kristensen, K., Cui, T., Zhang, H., Gold, A., Glasius, M., and Surratt, J. D.: Dimers in α-pinene secondary

497   organic aerosol: effect of hydroxyl radical, ozone, relative humidity and aerosol acidity, Atmos. Chem.

498   Phys., 14, 4201-4218, https://doi.org/10.5194/acp-14-4201-2014, 2014.

499   Kroll, J. H., Ng, N. L., Murphy, S. M., Varutbangkul, V., Flagan, R. C., and Seinfeld, J. H.: Chamber

500   studies of secondary organic aerosol growth by reactive uptake of simple carbonyl compounds, J.

Geophys. Res.-Atmos., 110, 10.1029/2005JD006004, 2005.

Kumar, M., Busch, D. H., Subramaniam, B., and Thompson, W. H.: Role of tunable acid catalysis in decomposition of α-Hydroxyalkyl hydroperoxides and mechanistic implications for tropospheric chemistry, J. Phys. Chem. A, 118, 9701-9711, https://doi.org/10.1021/jp505100x, 2014.

Leungsakul, S., Jaoui, M., and Kamens, R. M.: Kinetic Mechanism for Predicting Secondary Organic Aerosol Formation from the Reaction of d-Limonene with Ozone, Environ. Sci. Technol., 39, 9583-9594, https://doi.org/10.1021/es0492687, 2005.

Levy, H., II, Horowitz, L. W., Schwarzkopf, M. D., Ming, Y., Golaz, J.-C., Naik, V., and Ramaswamy, V.: The roles of aerosol direct and indirect effects in past and future climate change, J. Geophys. Res.-Atmos., 118, 4521-4532, https://doi.org/10.1002/jgrd.50192, 2013.

Li, J. Y., Zhang, H. W., Ying, Q., Wu, Z. J., Zhang, Y. L., Wang, X. M., Li, X. H., Sun, Y. L., Hu, M., Zhang, Y. H., and Hu, J. L.: Impacts of water partitioning and polarity of organic compounds on secondary organic aerosol over eastern China, Atmos. Chem. Phys., 20, 7291-7306, https://doi.org/10.5194/acp-20-7291-2020, 2020.

Li, K., Liggio, J., Lee, P., Han, C., Liu, Q., and Li, S.-M.: Secondary organic aerosol formation from α-pinene, alkanes, and oil-sands-related precursors in a new oxidation flow reactor, Atmos. Chem. Phys., 19, 9715-9731, https://doi.org/10.5194/acp-19-9715-2019, 2019a.

Li, X., Chee, S., Hao, J., Abbatt, J. P. D., Jiang, J., and Smith, J. N.: Relative humidity effect on the formation of highly oxidized molecules and new particles during monoterpene oxidation, Atmos. Chem. Phys., 19, 1555-1570, https://doi.org/10.5194/acp-19-1555-2019, 2019b.

Liu, Q., Liggio, J., Breznan, D., Thomson, E. M., Kumarathasan, P., Vincent, R., Li, K., and Li, S.-M.: Oxidative and Toxicological Evolution of Engineered Nanoparticles with Atmospherically Relevant Coatings, Environ. Sci. Technol., 53, 3058-3066, 10.1021/acs.est.8b06879, 2019.

Liu, Y., Liggio, J., Harner, T., Jantunen, L., Shoeib, M., and Li, S.-M.: Heterogeneous OH Initiated Oxidation: A Possible Explanation for the Persistence of Organophosphate Flame Retardants in Air, Environ. Sci. Technol., 48, 1041-1048, 10.1021/es404515k, 2014.

Ma, Y., Porter, R. A., Chappell, D., Russell, A. T., and Marston, G.: Mechanisms for the formation of organic acids in the gas-phase ozonolysis of 3-carene, Phys. Chem. Chem. Phys., 11, 4184-4197, https://doi.org/10.1039/b818750a, 2009.

530 Molteni, U., Bianchi, F., Klein, F., El Haddad, I., Frege, C., Rossi, M. J., Dommen, J., and Baltensperger,

531 U.: Formation of highly oxygenated organic molecules from aromatic compounds, Atmos. Chem. Phys.,

532 18, 1909-1921, https://doi.org/10.5194/acp-18-1909-2018, 2018.

533 Mot, M.-D., Gavrilaș, S., Lupitu, A. I., Moisa, C., Chambre, D., Tit, D. M., Bogdan, M. A., Bodescu, A.-

534 M., Copolovici, L., Copolovici, D. M., and Bungau, S. G.: Salvia officinalis L. essential oil:

535 characterization, antioxidant properties, and the effects of aromatherapy in adult patients, Antioxidants,

536 11, 808, https://doi.org/10.3390/antiox11050808, 2022.

537 Ng, N. L., Kroll, J. H., Chan, A. W. H., Chhabra, P. S., Flagan, R. C., and Seinfeld, J. H.: Secondary

538 organic aerosol formation from m-xylene, toluene, and benzene, Atmos. Chem. Phys., 7, 3909-3922,

539 https://doi.org/10.5194/acp-7-3909-2007, 2007.

540 Odum, J. R., Hoffmann, T., Bowman, F., Collins, D., Flagan, R. C., and Seinfeld, J. H.: Gas/particle

541 partitioning and secondary organic aerosol yields, Environ. Sci. Technol., 30, 2580-2585,

542 https://doi.org/10.1021/es950943+, 1996.

543 Palm, B. B., Campuzano-Jost, P., Ortega, A. M., Day, D. A., Kaser, L., Jud, W., Karl, T., Hansel, A.,

544 Hunter, J. F., Cross, E. S., Kroll, J. H., Peng, Z., Brune, W. H., and Jimenez, J. L.: In situ secondary

545 organic aerosol formation from ambient pine forest air using an oxidation flow reactor, Atmos. Chem.

546 Phys., 16, 2943-2970, https://doi.org/10.5194/acp-16-2943-2016, 2016.

547 Pathak, R. K., Salo, K., Emanuelsson, E. U., Cai, C., Lutz, A., Hallquist, A. M., and Hallquist, M.:

548 Influence of ozone and radical chemistry on limonene organic aerosol production and thermal

549 characteristics, Environ. Sci. Technol., 46, 11660-11669, https://doi.org/10.1021/es301750r, 2012.

550 Peng, Z., Lee-Taylor, J., Orlando, J. J., Tyndall, G. S., and Jimenez, J. L.: Organic peroxy radical

551 chemistry in oxidation flow reactors and environmental chambers and their atmospheric relevance,

552 Atmos. Chem. Phys., 19, 813-834, https://doi.org/10.5194/acp-19-813-2019, 2019.

553 Pye, H. O. T., Ward-Caviness, C. K., Murphy, B. N., Appel, K. W., and Seltzer, K. M.: Secondary organic

554 aerosol association with cardiorespiratory disease mortality in the United States, Nat. Commun., 12,

555 https://doi.org/10.1038/s41467-021-27484-1, 2021.

556 Ravichandran, C., Badgujar, P. C., Gundev, P., and Upadhyay, A.: Review of toxicological assessment of

557 d-limonene, a food and cosmetics additive, Food Chem. Toxicol., 120, 668-680,

558 https://doi.org/10.1016/j.fct.2018.07.052, 2018.

Sbai, S. E. and Farida, B.: Photochemical aging and secondary organic aerosols generated from limonene in an oxidation flow reactor, Environ. Sci. Pollut. Res., 26, 18411-18420, https://doi.org/10.1007/s11356-019-05012-5, 2019.

Seinfeld, J. H., Erdakos, G. B., Asher, W. E., and Pankow, J. F.: Modeling the formation of secondary organic aerosol (SOA). 2. The predicted effects of relative humidity on aerosol formation in the α-Pinene-, β-Pinene-, sabinene-, Δ^3-Carene-, and cyclohexene-ozone systems, Environ. Sci. Technol., 35, 1806-1817, https://doi.org/10.1021/es001765+, 2001.

Shaw, J. T., Lidster, R. T., Cryer, D. R., Ramirez, N., Whiting, F. C., Boustead, G. A., Whalley, L. K., Ingham, T., Rickard, A. R., Dunmore, R. E., Heard, D. E., Lewis, A. C., Carpenter, L. J., Hamilton, J. F., and Dillon, T. J.: A self-consistent, multivariate method for the determination of gas-phase rate coefficients, applied to reactions of atmospheric VOCs and the hydroxyl radical, Atmos. Chem. Phys., 18, 4039-4054, https://doi.org/10.5194/acp-18-4039-2018, 2018.

Shu, Y. G. and Atkinson, R.: RATE CONSTANTS FOR THE GAS-PHASE REACTIONS OF O-3 WITH A SERIES OF TERPENES AND OH RADICAL FORMATION FROM THE O-3 REACTIONS WITH SESQUITERPENES AT 296+/-2-K, INTERNATIONAL JOURNAL OF CHEMICAL KINETICS, 26, 1193-1205, 10.1002/kin.550261207, 1994.

Sindelarova, K., Granier, C., Bouarar, I., Guenther, A., Tilmes, S., Stavrakou, T., Müller, J. F., Kuhn, U., Stefani, P., and Knorr, W.: Global data set of biogenic VOC emissions calculated by the MEGAN model over the last 30 years, Atmos. Chem. Phys., 14, 9317-9341, https://doi.org/10.5194/acp-14-9317-2014, 2014.

Sun, Y., Wang, Z., Fu, P., Jiang, Q., Yang, T., Li, J., and Ge, X.: The impact of relative humidity on aerosol composition and evolution processes during wintertime in Beijing, China, Atmos. Environ., 77, 927-934, https://doi.org/10.1016/j.atmosenv.2013.06.019, 2013.

Thomsen, D., Elm, J., Rosati, B., Skonager, J. T., Bilde, M., and Glasius, M.: Large discrepancy in the formation of secondary organic aerosols from structurally similar monoterpenes, ACS Earth Space Chem., 5, 632-644, https://doi.org/10.1021/acsearthspacechem.0c00332, 2021.

Varutbangkul, V., Brechtel, F. J., Bahreini, R., Ng, N. L., Keywood, M. D., Kroll, J. H., Flagan, R. C., Seinfeld, J. H., Lee, A., and Goldstein, A. H.: Hygroscopicity of secondary organic aerosols formed by oxidation of cycloalkenes, monoterpenes, sesquiterpenes, and related compounds, Atmos. Chem. Phys.,

6, 2367-2388, https://doi.org/10.5194/acp-6-2367-2006, 2006.

Wang, L., Liu, Y., and Wang, L.: Ozonolysis of 3-carene in the atmosphere. Formation mechanism of hydroxyl radical and secondary ozonides, Phys. Chem. Chem. Phys., 21, 8081-8091, 10.1039/c8cp07195k, 2019.

Wang, L. Y. and Wang, L. M.: The oxidation mechanism of gas-phase ozonolysis of limonene in the atmosphere, Phys. Chem. Chem. Phys., 23, 9294-9303, https://doi.org/10.1039/d0cp05803c, 2021.

Watne, A. K., Westerlund, J., Hallquist, A. M., Brune, W. H., and Hallquist, M.: Ozone and OH-induced oxidation of monoterpenes: Changes in the thermal properties of secondary organic aerosol (SOA), J. Aerosol Sci, 114, 31-41, https://doi.org/10.1016/j.jaerosci.2017.08.011, 2017.

Xu, L., Tsona, N. T., and Du, L.: Relative humidity changes the role of SO_2 in biogenic secondary organic aerosol formation, J. Phys. Chem. Lett., 12, 7365-7372, https://doi.org/10.1021/acs.jpclett.1c01550, 2021.

Ye, J., Abbatt, J. P. D., and Chan, A. W. H.: Novel pathway of SO_2 oxidation in the atmosphere: reactions with monoterpene ozonolysis intermediates and secondary organic aerosol, Atmos. Chem. Phys., 18, 5549-5565, https://doi.org/10.5194/acp-18-5549-2018, 2018.

Yu, K. P., Lin, C. C., Yang, S. C., and Zhao, P.: Enhancement effect of relative humidity on the formation and regional respiratory deposition of secondary organic aerosol, J. Hazard. Mater., 191, 94-102, https://doi.org/10.1016/j.jhazmat.2011.04.042, 2011.

Zhang, H., Wang, S., Hao, J., Wang, X., Wang, S., Chai, F., and Li, M.: Air pollution and control action in Beijing, J. Clean Prod., 112, 1519-1527, https://doi.org/10.1016/j.jclepro.2015.04.092, 2016.

Zhang, Y., He, L., Sun, X., Ventura, O. N., and Herrmann, H.: Theoretical Investigation on the Oligomerization of Methylglyoxal and Glyoxal in Aqueous Atmospheric Aerosol Particles, ACS Earth Space Chem., 6, 1031-1043, 10.1021/acsearthspacechem.1c00422, 2022.

Zhao, R. R., Zhang, Q. X., Xu, X. Z., Zhao, W. X., Yu, H., Wang, W. J., Zhang, Y. M., and Zhang, W. J.: Effect of experimental conditions on secondary organic aerosol formation in an oxidation flow reactor, Atmos. Pollut. Res., 12, 392-400, https://doi.org/10.1016/j.apr.2021.01.011, 2021.

Ziemann, P. J. and Atkinson, R.: Kinetics, products, and mechanisms of secondary organic aerosol formation, Chem. Soc. Rev., 41, 6582-6605, https://doi.org/10.1039/c2cs35122f, 2012.

Supplement of

Contrasting impacts of humidity on the ozonolysis of monoterpenes: insights into the multi-generation chemical mechanism

Shan Zhang et al.

Correspondence to: Lin Du (lindu@sdu.edu.cn) and Kun Li (kun.li@sdu.edu.cn)

Section S1. Calculation of equivalent aging days

The equivalent aging days can be calculated by $\text{Age (days)} = k\frac{O_{3exp}}{[O_3]} = k\frac{[O_3]_0 \times RT}{[O_3]}$, where $[O_3]_0$ is the

initial ozone concentration in OFR, RT is the residence time, k is a constant coefficient which is equals

to 1.03 and $[O_3]$ is the mean ozone concentration in the atmosphere for 1 day, estimated to be 6.05×10^{16}

molec cm^{-3} s (Sbai and Farida, 2019).

Limonene (>99%, TCI), Δ^3-carene (>97%, Sigma Aldrich), methanol (Optima® LC-MS grade,

Fisher Scientific), formic acid (Optima® LC-MS grade, Fisher Scientific), pressured nitrogen gas

(99.999%, DEYI) were directly used for nitrogen-blowing without further purification. Ultrapure water

with a resistivity of 18.2 MΩ cm was generated with a water purification system (Millipore, France).

Section S3. Calculation of the pure-compound saturation concentrations

The pure-compound saturation concentrations (C_0) of SOA from limonene and Δ^3-carene have been

predicted using the following nonlinear expression (Li et al., 2016):

$$\text{Log}_{10}C_0 = \left(n_C^0 - n_C\right)b_C - n_O b_O - 2\frac{n_C n_O}{n_C + n_O}b_{CO}$$

The four free parameters n_C^0, b_C, b_O and b_{CO} represent the carbon number of 1 μg m^{-3} alkane, the

carbon-carbon interaction term, the oxygen-oxygen interaction term and the carbon-oxygen nonideality

respectively. The two independent variates n_C and n_O are the numbers of carbon and oxygen,

respectively. Based on the calculated saturation mass concentration of organic aerosols, they can be

classified into five groups (Donahue et al., 2012): extremely low-volatile organic compound (ELVOC;

$C_0 < 3 \times 10^{-4}$ μg m^{-3}); low-volatile organic compound (LVOC; $3 \times 10^{-4} < C_0 < 0.3$ μg m^{-3}); semi-volatile

organic compound (SVOC; $0.3 < C_0 < 300$ μg m^{-3}); intermediate volatility organic compound (IVOC;

$300 < C_0 < 3 \times 10^6$ μg m^{-3}) and volatile organic compounds (VOC; $C_0 > 3 \times 10^6$ μg m^{-3}).

Table S1. The number and intensity proportion of four groups for limonene

Groups	Monomers	Dimers	Trimers	Tetramers
Number (L)[a]	242	162	122	116
Number (H)[b]	272	187	134	105
Intensity proportion (L)[a]	61.8%	25.7%	9.4%	3.1%
Intensity proportion (H)[b]	65.6%	24.4%	7.9%	2.0%

[a] L means under low RH. [b] H means under high RH.

Table S2. The number and intensity proportion of four groups for Δ^3-carene

Groups	Monomers	Dimers	Trimers	Tetramers
Number (L)[a]	239	178	76	4
Number (H)[b]	216	151	26	1
Intensity proportion (L)[a]	69.8%	28.6%	1.6%	0.5%
Intensity proportion (H)[b]	72.5%	26.9%	2.0%	0.2%

[a] L means under low RH. [b] H means under high RH.
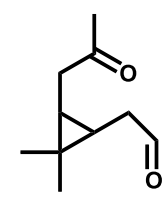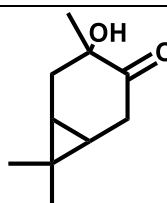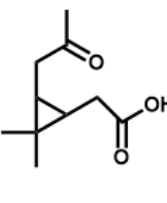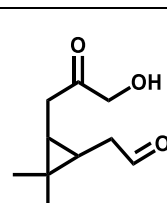
Table S3. Intensity and partitioning coefficient for limonene products identified by MS (can be found in the proposed mechanism).

	Molecular formula	Low RH		High RH		Partitioning coefficient	
		Absolute intensity	Relative intensity	Absolute intensity	Relative intensity	Low RH	High RH
Monomers	$C_{10}H_{16}O_2$	9.01×10^2	1.72×10^{-4}	1.27×10^3	1.42×10^{-4}	0.01	0.02
	$C_9H_{14}O_3$	1.49×10^4	2.85×10^{-3}	3.00×10^4	3.33×10^{-3}	0.02	0.05
	$C_{10}H_{16}O_3$	4.99×10^4	9.54×10^{-3}	8.58×10^4	9.55×10^{-3}	0.05	0.10
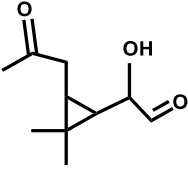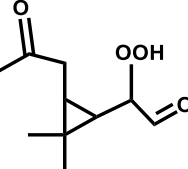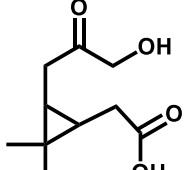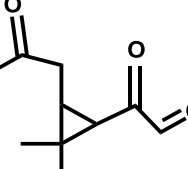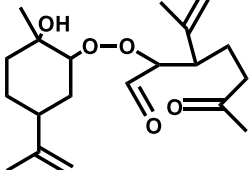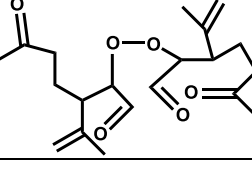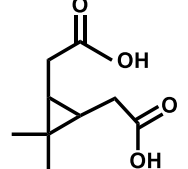
	Formula						
	$C_9H_{14}O_4$	1.29×10^5	2.46×10^{-2}	2.46×10^5	2.73×10^{-2}	0.13	0.25
	$C_{10}H_{18}O_3$	1.21×10^3	2.31×10^{-4}	1.64×10^3	1.82×10^{-4}	0.05	0.10
	$C_9H_{16}O_4$	7.60×10^3	1.45×10^{-3}	1.51×10^4	1.68×10^{-3}	0.13	0.25
	$C_{10}H_{16}O_4$	1.28×10^5	2.45×10^{-2}	2.24×10^5	2.49×10^{-2}	0.24	0.41
	$C_9H_{14}O_5$	1.28×10^5	2.45×10^{-2}	2.08×10^5	2.33×10^{-2}	0.58	0.76
	$C_9H_{14}O_3$	1.49×10^4	2.85×10^{-3}	3.00×10^4	-	0.02	0.05
	$C_8H_{12}O_4$	6.71×10^4	1.28×10^{-2}	1.35×10^5	-	0.07	0.15
	$C_{10}H_{18}O_2$	2.62×10^2	5.01×10^{-5}	4.60×10^2	5.12×10^{-5}	0.01	0.02
	$C_9H_{16}O_3$	7.20×10^3	1.38×10^{-3}	1.48×10^4	1.64×10^{-3}	0.02	0.05
	$C_{10}H_{14}O_3$	7.34×10^3	1.40×10^{-3}	1.34×10^4	1.50×10^{-3}	0.05	0.10
	$C_9H_{12}O_4$	3.49×10^4	6.66×10^{-3}	5.94×10^4	6.61×10^{-3}	0.13	0.25
	$C_{10}H_{14}O_5$	4.00×10^4	7.64×10^{-3}	5.44×10^4	6.06×10^{-3}	0.71	0.85
	$C_9H_{12}O_6$	1.25×10^4	2.38×10^{-3}	2.08×10^4	2.31×10^{-3}	0.94	0.97
	$C_{10}H_{16}O_6$	-	8.32×10^{-3}	7.12×10^4	7.93×10^{-3}	0.96	0.98
	$C_{10}H_{18}O_4$	-	1.49×10^{-3}	1.29×10^5	1.44×10^{-3}	0.24	0.41
	$C_9H_{16}O_5$	1.40×10^4	2.67×10^{-3}	2.76×10^4	3.08×10^{-3}	0.58	0.76
	$C_{10}H_{18}O_6$	-	1.39×10^{-3}	1.31×10^5	1.46×10^{-3}	0.96	0.98
	$C_{10}H_{16}O_5$	8.02×10^3	1.53×10^{-2}	1.49×10^4	1.65×10^{-2}	0.72	0.85
	$C_9H_{14}O_6$	-	-	9.40×10^4	1.05×10^{-2}	0.94	0.97
	$C_{10}H_{18}O_5$	9.05×10^3	1.73×10^{-3}	1.65×10^4	1.84×10^{-3}	0.72	0.85
	$C_9H_{16}O_6$	-	-	1.41×10^4	1.57×10^{-3}	0.94	0.97
HOMs	$C_9H_{14}O_7$	-	4.19×10^{-3}	4.44×10^4	4.95×10^{-3}	1.00	1.00
	$C_{10}H_{14}O_7$	8.75×10^3	1.67×10^{-3}	1.32×10^4	1.47×10^{-3}	1.00	1.00
	$C_{10}H_{14}O_{11}$	-	-	3.68×10^2	4.10×10^{-5}	1.00	1.00
	$C_{10}H_{14}O_{13}$	-	-	3.88×10^2	4.32×10^{-5}	1.00	1.00
	$C_9H_{16}O_7$	7.71×10^3	1.47×10^{-3}	1.91×10^4	2.13×10^{-3}	1.00	1.00
	$C_{10}H_{16}O_7$	1.63×10^4	3.12×10^{-3}	3.00×10^4	3.35×10^{-3}	1.00	1.00
	$C_9H_{14}O_8$	-	-	4.12×10^3	4.60×10^{-4}	1.00	1.00
	$C_{10}H_{18}O_7$	4.70×10^3	8.99×10^{-4}	8.90×10^3	9.91×10^{-4}	1.00	1.00

	$C_9H_{16}O_8$	-	-	2.54×10^3	2.82×10^{-4}	1.00	1.00
	$C_{10}H_{16}O_8$	3.63×10^3	6.94×10^{-4}	7.08×10^3	7.67×10^{-4}	1.00	1.00
Dimers	$C_{20}H_{34}O_4$	-		4.98×10^2	5.55×10^{-5}	1.00	1.00
	$C_{18}H_{30}O_6$	-	-	2.74×10^3	3.04×10^{-4}	1.00	1.00
	$C_{18}H_{28}O_7$	-	-	1.53×10^4	1.70×10^{-3}	1.00	1.00
	$C_{20}H_{30}O_8$	3.61×10^2	1.97×10^{-4}	1.25×10^4	1.40×10^{-3}	1.00	1.00
	$C_{18}H_{26}O_8$	1.29×10^4	2.47×10^{-3}	2.34×10^4	2.62×10^{-3}	1.00	1.00
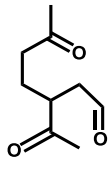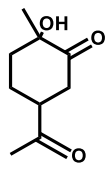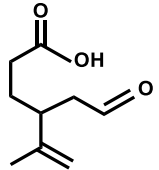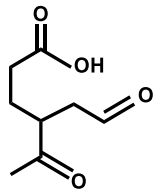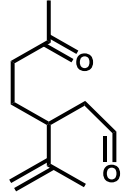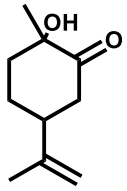
Table S4. Δ^3-carene-SOA identified under high RH in Fig. S3.
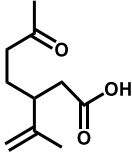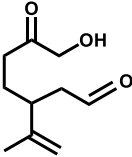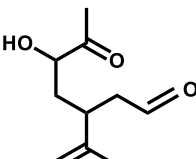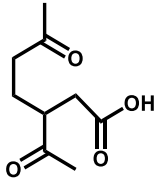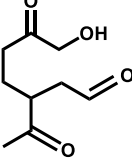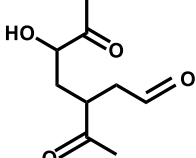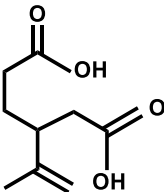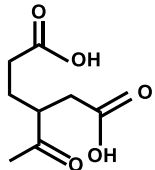
[M–H]-	Theo. Mass	Error (ppm)	DBE	Suggested Formula	Molecular Structure
167.10657	167.107753	7.081	3	$C_{10}H_{16}O_2$	
183.101733	183.102668	5.105	3	$C_{10}H_{16}O_3$	
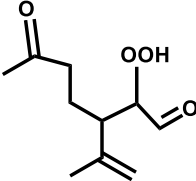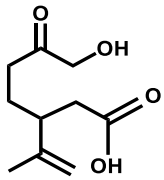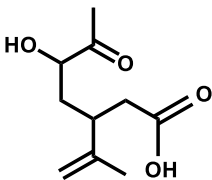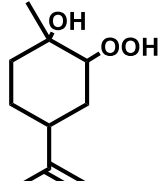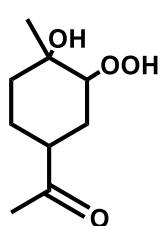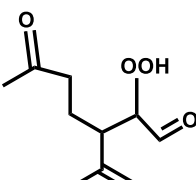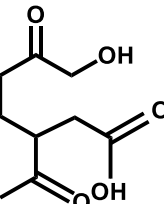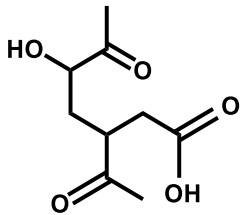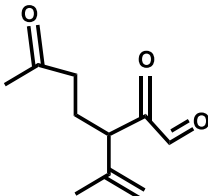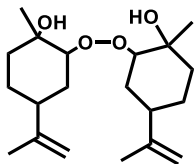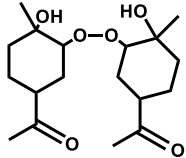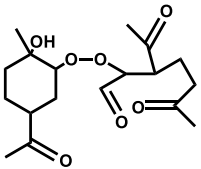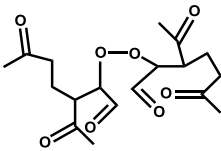
169.122233	169.123403	6.921	2	$C_{10}H_{18}O_2$	
199.096239	199.097583	6.747	3	$C_{10}H_{16}O_4$	
181.085655	181.087018	7.526	3	$C_{10}H_{14}O_3$	
351.214938	351.217698	7.858	5	$C_{20}H_{32}O_5$	
365.194982	365.196962	5.421	6	$C_{20}H_{30}O_6$	
185.080938	185.081932	5.374	3	$C_9H_{14}O_4$	

Table S5. Limonene-SOA under high RH identified in Fig. 3 and Fig. 4.

[M–H]⁻	Theo. Mass	Error (ppm)	DBE	Suggested Formula	Molecular Structure
169.086288	169.087018	4.319	3	$C_9H_{14}O_3$	
183.065329	183.066282	5.208	4	$C_9H_{12}O_4$	
167.107219	167.107753	3.198	2	$C_{10}H_{16}O_2$	

183.102508	183.102668	0.874	3	$C_{10}H_{16}O_3$	
185.081203	185.081932	3.943	3	$C_9H_{14}O_4$	
187.060122	187.061197	5.749	3	$C_8H_{12}O_5$	

199.096857	199.097583	3.644	3	$C_{10}H_{16}O_4$	
185.117126	185.118318	6.441	2	$C_{10}H_{18}O_3$	
187.096428	187.097583	6.172	2	$C_9H_{16}O_4$	
201.075661	201.076847	5.896	3	$C_9H_{14}O_5$	

181.086015	181.087018	5.536	4	$C_{10}H_{14}O_3$	
337.237472	337.238433	2.851	4	$C_{20}H_{34}O_4$	
341.196189	341.196962	2.266	4	$C_{18}H_{30}O_6$	
355.17525	355.176227	2.749	5	$C_{18}H_{28}O_7$	
369.154689	369.155491	2.174	6	$C_{18}H_{26}O_8$	

54 dimers exclusively detected under high RH (limonene)	63 dimers exclusively detected under low RH (Δ^3-carene)

Molecular formula	Absolute intensity (High RH)	Molecular formula	Absolute intensity (Low RH)
$C_{18}H_{26}O_4$	4.66×10^2	$C_{17}H_{24}O_5$	1.59×10^3
$C_{16}H_{20}O_6$	7.24×10^2	$C_{10}H_{14}O_{11}$	3.90×10^3
$C_{13}H_{18}O_9$	3.36×10^2	$C_{14}H_{14}O_8$	4.02×10^3
$C_{17}H_{22}O_6$	6.63×10^3	$C_{20}H_{40}O_2$	4.60×10^3
$C_{18}H_{26}O_5$	6.28×10^2	$C_{12}H_{10}O_{10}$	4.00×10^3
$C_{19}H_{32}O_4$	1.58×10^3	$C_{13}H_{16}O_9$	8.34×10^3
$C_{15}H_{18}O_8$	1.65×10^3	$C_{19}H_{26}O_4$	4.96×10^3
$C_{13}H_{12}O_{10}$	8.85×10^3	$C_{17}H_{22}O_6$	1.05×10^3
$C_{14}H_{20}O_9$	8.44×10^2	$C_{13}H_{12}O_{10}$	5.46×10^3
$C_{16}H_{28}O_7$	9.89×10^3	$C_{13}H_{18}O_{10}$	4.68×10^3
$C_{15}H_{26}O_8$	2.18×10^3	$C_{15}H_{12}O_9$	4.22×10^3
$C_{10}H_8O_{13}$	6.33×10^3	$C_{10}H_{12}O_{13}$	5.00×10^3
$C_{18}H_{24}O_6$	6.06×10^2	$C_{22}H_{28}O_3$	8.88×10^3
$C_{11}H_{14}O_{12}$	7.70×10^2	$C_{19}H_{26}O_6$	1.54×10^3
$C_{21}H_{22}O_4$	4.80×10^3	$C_{16}H_{20}O_9$	1.64×10^3
C20H34O4	2.53×10^3	$C_{15}H_{18}O_{10}$	5.00×10^3
$C_{23}H_{32}O_2$	2.12×10^3	$C_{16}H_{22}O_9$	1.69×10^3
$C_{18}H_{32}O_6$	3.68×10^2	$C_{18}H_{22}O_8$	3.32×10^3
$C_{17}H_{30}O_7$	7.46×10^3	$C_{12}H_{16}O_{13}$	4.00×10^3
$C_{14}H_{22}O_{10}$	4.04×10^3	$C_{20}H_{32}O_6$	8.21×10^3
$C_{21}H_{36}O_4$	1.36×10^4	$C_{16}H_{18}O_{10}$	4.50×10^3
$C_{17}H_{30}O_8$	4.68×10^2	$C_{16}H_{20}O_{10}$	5.20×10^3
$C_{12}H_{16}O_{13}$	2.43×10^3	$C_{19}H_{24}O_8$	8.21×10^3
$C_{11}H_{14}O_{14}$	4.46×10^2	$C_{20}H_{28}O_7$	2.38×10^3
$C_{18}H_{30}O_8$	4.46×10^2	$C_{17}H_{20}O_{10}$	4.16×10^3
$C_{16}H_{26}O_{10}$	7.44×10^2	$C_{21}H_{36}O_6$	8.03×10^3
$C_{17}H_{20}O_{10}$	2.12×10^3	$C_{16}H_{26}O_{11}$	1.16×10^3
$C_{16}H_{24}O_{11}$	1.48×10^3	$C_{17}H_{26}O_{11}$	1.32×10^3
$C_{20}H_{24}O_8$	3.96×10^3	$C_{18}H_{18}O_{11}$	4.02×10^3
$C_{17}H_{22}O_{11}$	2.48×10^3	$C_{18}H_{22}O_{11}$	4.54×10^3
$C_{21}H_{34}O_8$	1.28×10^4	$C_{18}H_{26}O_{11}$	1.49×10^3
$C_{13}H_{22}O_{15}$	4.06×10^2	$C_{22}H_{28}O_8$	4.62×10^3
$C_{19}H_{32}O_{10}$	5.30×10^2	$C_{15}H_{18}O_{14}$	4.08×10^3
$C_{22}H_{32}O_8$	5.90×10^3	$C_{20}H_{32}O_{10}$	5.97×10^3
$C_{20}H_{28}O_{10}$	1.53×10^3	$C_{17}H_{22}O_{13}$	5.10×10^3
$C_{18}H_{18}O_{13}$	4.49×10^3	$C_{21}H_{28}O_{10}$	4.25×10^3
$C_{19}H_{24}O_{12}$	1.49×10^4	$C_{19}H_{22}O_{12}$	5.44×10^3
$C_{19}H_{30}O_{12}$	6.10×10^2	$C_{22}H_{34}O_9$	7.52×10^3
$C_{15}H_{18}O_{16}$	1.14×10^3	$C_{21}H_{34}O_{10}$	2.12×10^3
$C_{23}H_{38}O_9$	4.34×10^2	$C_{14}H_{24}O_{16}$	4.80×10^3
$C_{32}H_{44}O_2$	8.96×10^2	$C_{15}H_{22}O_{16}$	4.04×10^3

Molecular formula	Intensity	Molecular formula	Intensity
$C_{21}H_{36}O_{11}$	3.74×10^2	$C_{17}H_{30}O_{14}$	3.51×10^3
$C_{14}H_{26}O_{17}$	1.00×10^3	$C_{22}H_{36}O_{10}$	4.02×10^3
$C_{20}H_{26}O_{13}$	1.26×10^4	$C_{18}H_{24}O_{14}$	4.44×10^3
$C_{22}H_{34}O_{11}$	1.92×10^3	$C_{19}H_{28}O_{13}$	6.68×10^3
$C_{20}H_{30}O_{13}$	9.36×10^2	$C_{20}H_{22}O_{13}$	3.90×10^3
$C_{18}H_{24}O_{15}$	2.05×10^3	$C_{21}H_{26}O_{12}$	4.48×10^3
$C_{21}H_{38}O_{12}$	9.16×10^2	$C_{22}H_{30}O_{11}$	2.29×10^3
$C_{24}H_{38}O_{10}$	3.78×10^3	$C_{15}H_{24}O_{17}$	4.70×10^3
$C_{16}H_{24}O_{17}$	1.26×10^3	$C_{25}H_{38}O_{9}$	5.24×10^3
$C_{21}H_{24}O_{14}$	4.80×10^3	$C_{17}H_{26}O_{16}$	5.18×10^3
$C_{20}H_{34}O_{4}$	4.98×10^2	$C_{21}H_{26}O_{13}$	4.82×10^3
$C_{18}H_{30}O_{6}$	2.74×10^3	$C_{22}H_{30}O_{12}$	2.47×10^3
$C_{18}H_{28}O_{7}$	1.53×10^4	$C_{16}H_{24}O_{17}$	5.16×10^3
		$C_{17}H_{28}O_{16}$	6.58×10^3
		$C_{29}H_{44}O_{6}$	5.82×10^3
		$C_{17}H_{30}O_{16}$	2.06×10^3
		$C_{22}H_{38}O_{12}$	3.86×10^3
		$C_{16}H_{32}O_{17}$	7.04×10^3
		$C_{23}H_{30}O_{12}$	1.26×10^3
		$C_{24}H_{34}O_{11}$	6.82×10^3
		$C_{20}H_{30}O_{10}$	4.14×10^3
		$C_{20}H_{32}O_{11}$	3.41×10^3

Table S7. Intensity and partitioning coefficient for Δ^3-carene products identified by MS (can be found in the proposed mechanism).

	Molecular formula	Low RH		High RH		Partitioning coefficient	
		Absolute intensity	Relative intensity	Absolute intensity	Relative intensity	Low RH	High RH
HOMs	$C_{10}H_{14}O_{11}$	3.41×10^2	5.44×10^{-5}	-	-	1.00	1.00
	$C_{10}H_{16}O_{8}$	1.42×10^3	2.26×10^{-4}	8.31×10^2	1.89×10^{-4}	1.00	1.00
	$C_{10}H_{18}O_{11}$	2.32×10^3	3.70×10^{-4}	1.61×10^3	3.65×10^{-4}	1.00	1.00
	$C_{10}H_{18}O_{8}$	4.60×10^2	7.34×10^{-5}	-	-	1.00	1.00
Dimers	$C_{20}H_{30}O_{6}$	1.25×10^4	1.97×10^{-3}	7.55×10^3	1.71×10^{-3}	1.00	1.00
	$C_{20}H_{30}O_{8}$	6.99×10^3	1.11×10^{-3}	4.16×10^3	9.44×10^{-4}	1.00	1.00
	$C_{20}H_{30}O_{10}$	3.62×10^3	5.77×10^{-4}	-	-	1.00	1.00

$C_{20}H_{32}O_7$	1.58×10^4	2.51×10^{-3}	7.45×10^3	1.69×10^{-3}	1.00	1.00
$C_{20}H_{32}O_9$	1.31×10^4	2.09×10^{-3}	8.76×10^3	1.99×10^{-3}	1.00	1.00
$C_{20}H_{32}O_{11}$	2.98×10^3	4.76×10^{-4}	-	-	1.00	1.00
$C_{20}H_{32}O_{13}$	5.11×10^2	8.15×10^{-5}	3.12×10^2	7.09×10^{-5}	1.00	1.00

Table S8. The experimental data and results of β-caryophyllene oxidation.

Exp.	[Precursor] (ppb)	[O]₃ (ppm)	T (K)	RH (%)	$N_{(14.1\text{-}735nm)}$[a] (no.cm⁻³)	$M_{(14.1\text{-}735nm)}$[b] (μg m⁻³)	$D_{(mean)}$[c] (nm)	SOA yield (%)
1	234.9	6.3	298	3.2	$(2.3\pm0.1)\times10^6$	168.2 ± 13.8	49.9 ± 2.5	9.4 ± 0.8
2	255.3	6.4	298	58	$(3.6\pm0.5)\times10^6$	584.1 ± 10.9	64.3 ± 0.7	25.1 ± 0.5

[a] $N_{(14.1\text{-}735\ nm)}$ means the total particle number concentration from size 13.8 nm to 723.4 nm. [b] $M_{(13.8\text{-}723.4\ nm)}$ means the total particle mass concentration from size 13.8 nm to 723.4 nm. [c] $D_{(mean)}$ means the particle mean diameter.
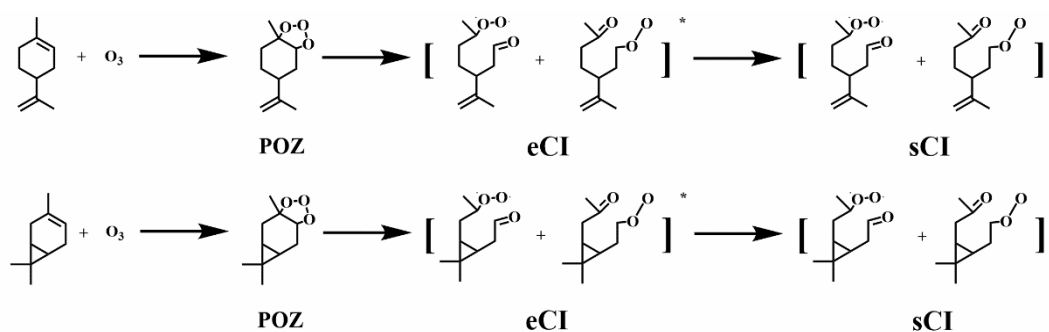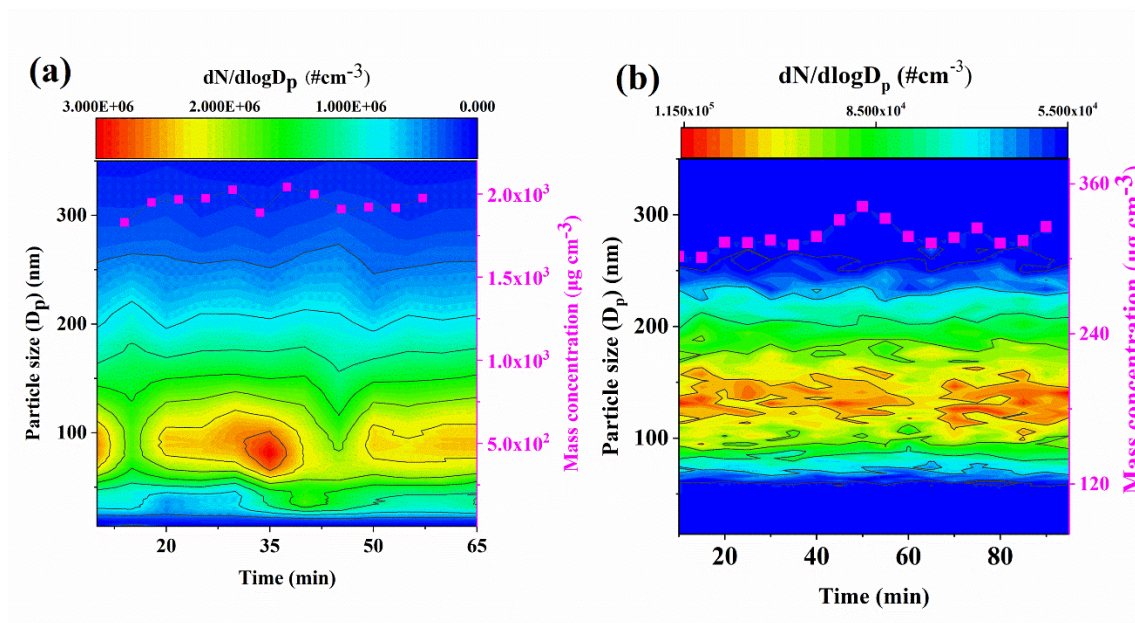

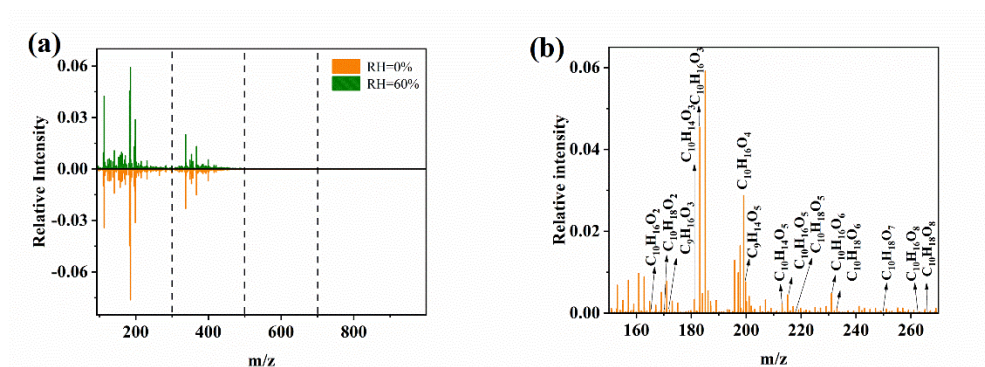**Fig S1.** The formation of sCIs from the ozonolysis of limonene and Δ^3-carene.
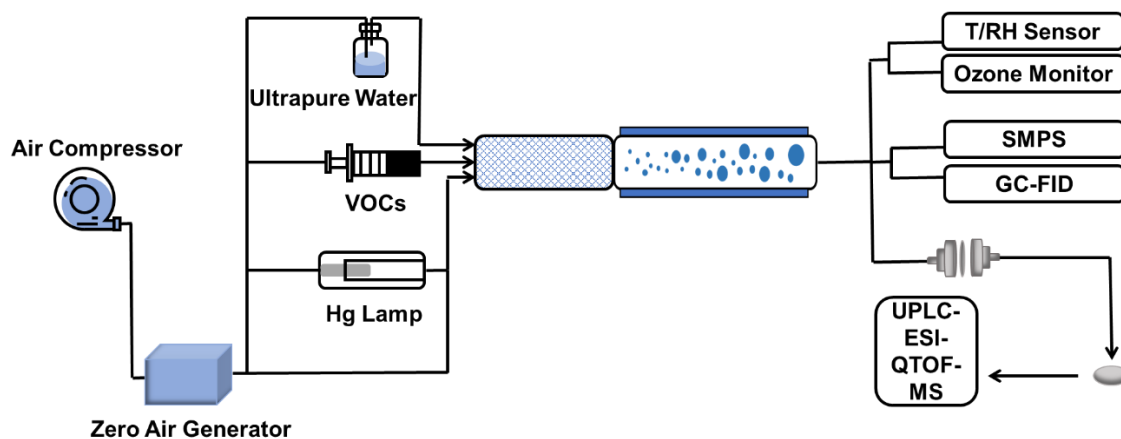
Figure S3. Time evolution of SOA size (electromobility diameter) and mass concentration obtained from limonene/O_3 and Δ^3-carene/O_3 experiments (Exp. 6 and Exp. 11).


Fig. S4. UPLC/ (−) ESI-Q-TOF-MS mass spectra of SOA from Δ^3-carene ozonolysis. (a) MS under high and low RH conditions; (b) the identification of monomers under low RH condition.
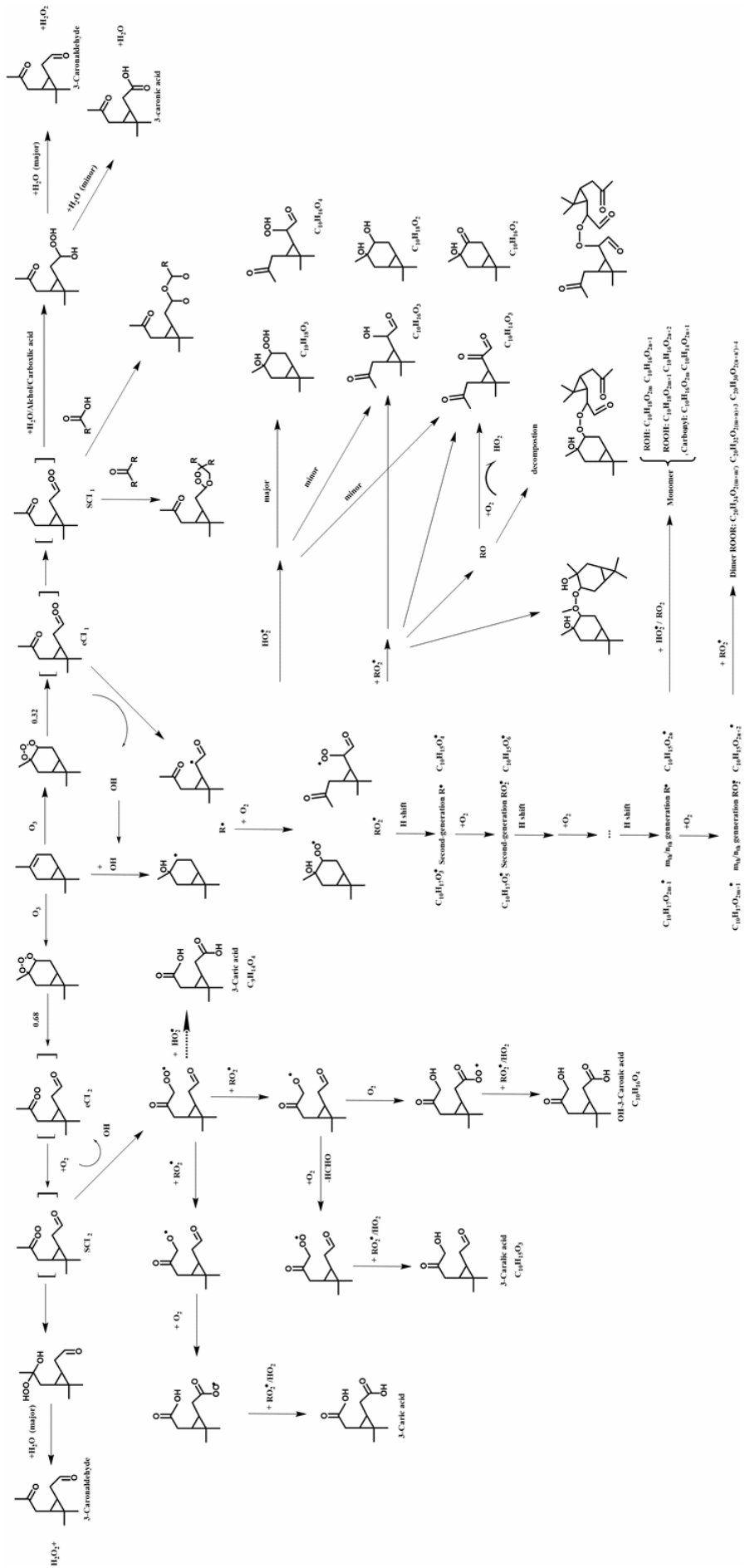
Figure S5. Proposed formation mechanisms for SOA formation from Δ^3-carene ozonolysis under high RH.
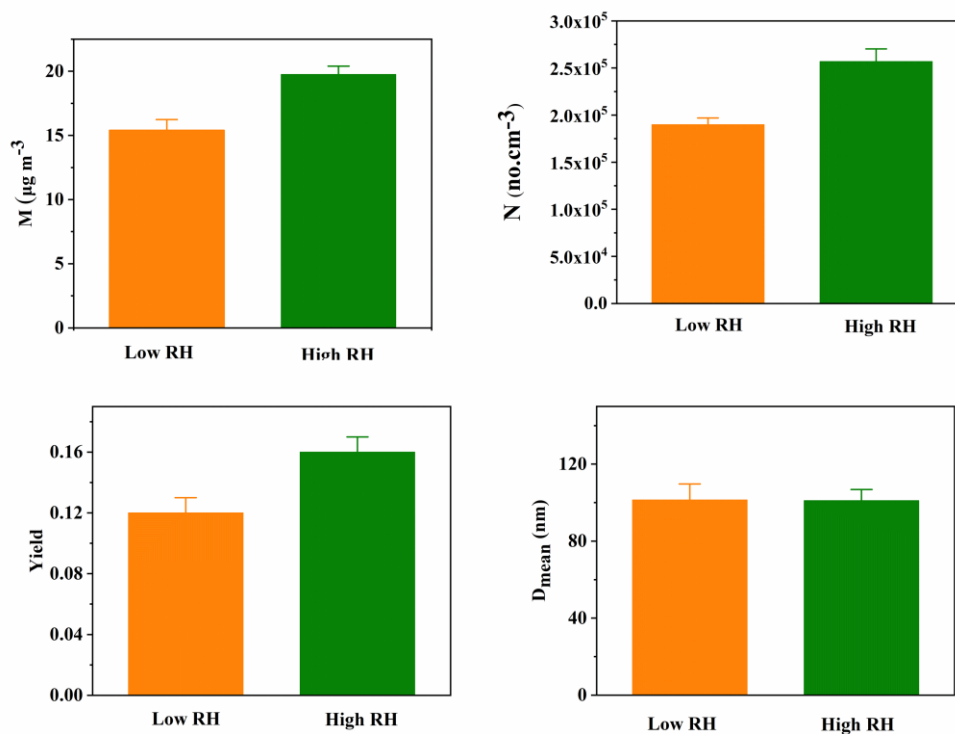
Figure S6. The SOA formation of low-concentration limonene under low and high RH (a) mass concentration (b) number concentration (c) SOA yield (d) mean diameter.
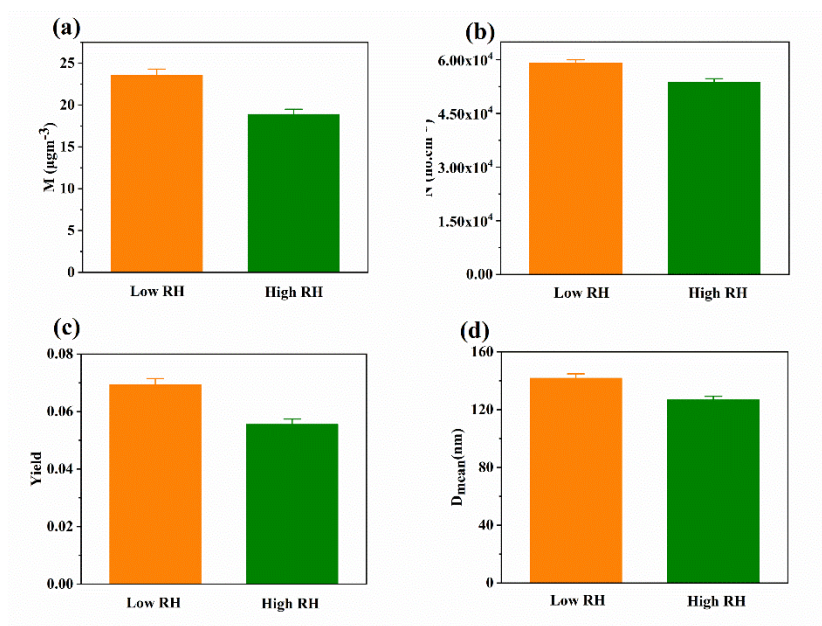
Figure S7. The SOA formation from endocyclic ozonolysis of limonene under low and high RH (a) mass concentration (b) number concentration (c) SOA yield (d) mean diameter. The initial concentration of limonene is 450 ppb and the concentration of O_3 is 67 ppb. Limonene ozonolysis primarily took place on endo-double bonds, with a rate constant of 2.01×10^{-16} cm^3 molec.$^{-1}$ s^{-1} (Shu and Atkinson, 1994).
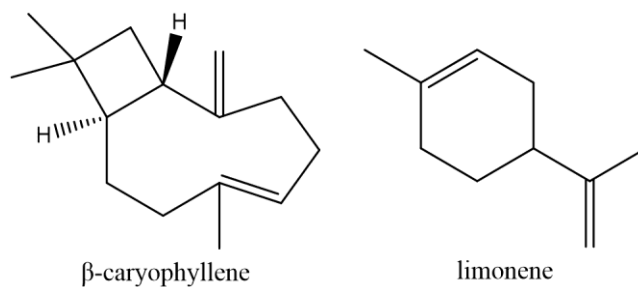
Figure S8. The molecular structure of β-caryophyllene and limonene.

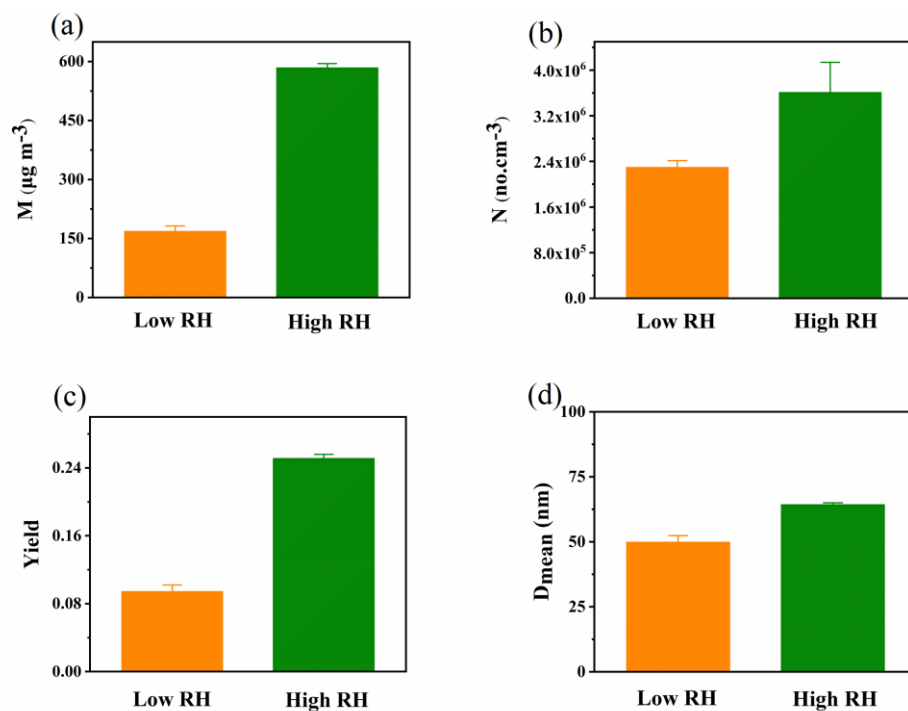**Figure S9.** The SOA formation of β-caryophyllene under low and high RH (a) mass concentration (b) number concentration (c) SOA yield (d) mean diameter.

Reference

Donahue, N. M., Kroll, J. H., Pandis, S. N., and Robinson, A. L.: A two-dimensional volatility basis set - Part 2: Diagnostics of organic-aerosol evolution, Atmos. Chem. Phys., 12, 615-634, https://doi.org/10.5194/acp-12-615-2012, 2012.

Li, Y., Poeschl, U., and Shiraiwa, M.: Molecular corridors and parameterizations of volatility in the chemical evolution of organic aerosols, Atmos. Chem. Phys., 16, 3327-3344, https://doi.org/10.5194/acp-16-3327-2016, 2016.

Sbai, S. E. and Farida, B.: Photochemical aging and secondary organic aerosols generated from limonene in an oxidation flow reactor, Environ. Sci. Pollut. Res., 26, 18411-18420, https://doi.org/10.1007/s11356-019-05012-5, 2019.

Shu, Y. G. and Atkinson, R.: RATE CONSTANTS FOR THE GAS-PHASE REACTIONS OF O-3 WITH A SERIES OF TERPENES AND OH RADICAL FORMATION FROM THE O-3 REACTIONS WITH SESQUITERPENES AT 296+/-2-K, INTERNATIONAL JOURNAL OF CHEMICAL KINETICS, 26, 1193-1205, 10.1002/kin.550261207, 1994.